Climate change impacts on conventional and flash droughts in the Mekong River Basin

Hyunwoo Kang, Venkataramana Sridhar *, Syed A. Ali

Department of Biological Systems Engineering, Virginia Polytechnic Institute and State University, Blacksburg, VA 24061, USA

HIGHLIGHTS

- Conventional and flash droughts assessments using simulated soil moisture-based drought indices
- Soil moisture is key source of discrepancy in predicting future conventional droughts.
- A range of flash droughts from SWAT (up to 165% increase) and VIC (up to −44% decrease) is plausible.
- Basin countries have differential impacts, so targeted future adaptation strategy is required.

GRAPHICAL ABSTRACT
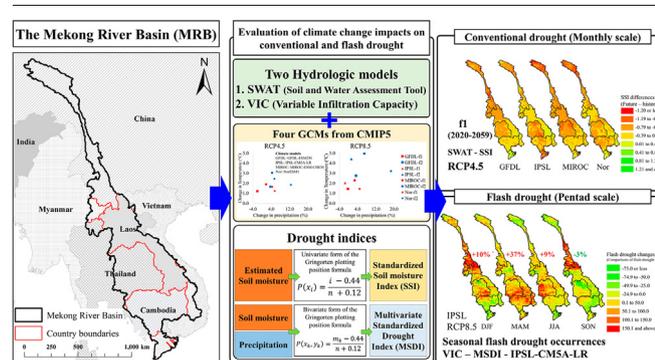
ABSTRACT

Recent drought events in the Mekong River Basin (MRB) have resulted in devastating environmental and economic losses, and climate change and human-induced alterations have exacerbated drought conditions. Using hydrologic models and multiple climate change scenarios, this study quantified the future climate change impacts on conventional and flash drought conditions in the MRB. The Soil and Water Assessment Tool (SWAT) and Variable Infiltration Capacity (VIC) models were applied to estimate long-term drought indices for conventional and flash drought conditions over historical and future periods (1966–2099), using two emission scenarios (RCP 4.5 and RCP8.5), and four climate models from the Coupled Model Intercomparison Project Phase 5 (CMIP5). For the conventional drought assessment, monthly scale drought indices were estimated, and pentad-scale (5 days) drought indices were computed for the flash drought evaluations. There were overall increases in droughts from the SWAT model for the conventional drought conditions and overall decreases from the VIC model. For the flash drought conditions, the SWAT-driven drought indices showed overall increases in drought occurrences (up to 165%). On the contrary, the VIC-driven drought indices presented decreases in drought occurrences (up to −44%). The conventional and flash drought evaluations differ between these models as they partition the water budget, specifically soil moisture differently. We conclude that the proposed framework, which includes hydrologic models, various emission scenarios, and projections, allows us to assess the various perspectives on drought conditions. Basin countries have differential impacts, so targeted future adaptation strategy is required.

1. Introduction

Drought is defined as a period in which a region experiences a lack of precipitation over an extended period of time. Drought is one of the most expensive natural hazards (Mishra and Singh, 2010) and it is widely recognized as an environmental disaster that has a negative impact on crop management, water resource, and various sectors of the economy (Mishra and Singh, 2010; Sheffield and Wood, 2012; Duan and Mei, 2014). Furthermore, drought is a destructive natural hazard that is linked to increased wildfire risk, crop losses, reduced power generation, food security, and indirect health effects (Westerling et al., 2006; Stanke et al., 2013;

Cheeseman, 2016). Over the last few decades, climate change and anthropogenic activities have exacerbated drought duration, frequency, and severity in many parts of the world, and severe drought events have had some devastating consequences (Trenberth et al., 2014; Sheffield et al., 2012; Mukherjee et al., 2018; Ahmadalipour et al., 2019). Moreover, water scarcity has worsened as a result of population growth and the expansion of the agricultural, energy, and industrial sectors (Mishra and Singh, 2010; Kang et al., 2019; Kang and Sridhar, 2019, 2020; Kang et al., 2021).

The Mekong River Basin (MRB) is a transboundary river basin that includes parts of the countries of China, Cambodia, Lao PDR, Myanmar, Thailand, and Vietnam, where extreme drought events have been common in recent few decades (Ruiz-Barradas and Nigam, 2018; Jing et al., 2020; Kang and Sridhar, 2021). For instance, the drought event of 1997–1998 caused an economic loss of 400 million USD in the agricultural sector in Vietnam (Shaw and Nguyen, 2011), and the 2004–2005 drought caused harm to all four countries in the Lower Mekong River Basin (LMB; Cambodia, Lao PDR, Thailand, and Vietnam) (Food and Agriculture Organization (FAO), 2005; WFP, 2009). Furthermore, there was an exceptional drought in 2015–2016; affecting more than 75% of the LMB (Guo et al., 2017), with estimated economic losses were 1.7 billion USD in Thailand (Wipatayotin, 2016) and 669 million USD in Vietnam (VNE, 2016). Moreover, the MRB experienced another catastrophic drought in 2019–2020, wreaking havoc on agricultural production and livelihood activities in the region (Keovilignavong et al., 2021). Numerous studies have indicated that some regions will face increasing extreme drought conditions in the future (Thilakarathne and Sridhar, 2017; Sam et al., 2019; Kang et al., 2021; Li et al., 2021).

Flash drought is a subset of droughts distinguished by a sudden onset and rapid intensification (Svoboda et al., 2002; Otkin et al., 2013). Continuous precipitation deficits are generally influencing the development of conventional droughts. However, other hydro-climatological factors such as abnormal heatwaves, low humidity, and strong winds, which result in increased evaporative demand and soil moisture depletion due to ET increases, generally influence the severity and rapid development of flash drought (Otkin et al., 2013; Anderson et al., 2013; Parker et al., 2021). If these climate anomalies persist for an extended period of time, they can deplete surface soil moisture, increase vegetation stress, and result in the rapid development of drought (Ford et al., 2015; Otkin et al., 2018; Christian et al., 2019). Flash drought was first investigated by Otkin et al. (2013, 2014) using the satellite-based evaporative stress index (ESI; Anderson et al., 2007), and it explored the relationship between rapid propagation of droughts and evaporative demands. In addition, the evaporative demand drought index (EDDI) has been developed and is used to assess flash droughts (Hobbins et al., 2016; McEvoy et al., 2016). Numerous studies have been conducted in many parts of the world to investigate various aspects of flash droughts under current and future conditions (Basara et al., 2019; Christian et al., 2019; Christian et al., 2020; Nguyen et al., 2019; Yuan et al., 2019; Noguera et al., 2021). However, only a limited study on the effects of climate change on the MRB is available.

Various drought indices have been developed and applied to evaluate different perspectives of droughts, including meteorological, agricultural, and hydrological droughts, and they are also used in MRB drought assessments. The Standardized Precipitation Index (McKee et al., 1993) is one of the most widely used indices for monitoring meteorological drought conditions, and is used in a variety of MRB drought assessments, including drought monitoring (Guo et al., 2017), climate change impacts on droughts (Li et al., 2021), and historical drought assessments (Zhang and Liu, 2020). The Standardized Soil Moisture Index (SSI; Hao and AghaKouchak, 2013, 2014) is based on the SPI concept, and the Multivariate Standardized Drought Index (MSDI) was developed to assess multivariate drought characteristics (Hao and AghaKouchak, 2013, 2014). The initial application of MSDI used a combination of precipitation and soil moisture. Furthermore, because MSDI is based on the joint distribution, multiple combinations of hydrometeorological variables are available (Hao and AghaKouchak,

2013). In this study, the SSI and MSDI were used to assess the effects of climate change on conventional (i.e., 12-month scale) and flash drought conditions.

Spatiotemporal variations of hydrometeorological variables are required to investigate and analyze the drought conditions (Sridhar et al., 2013; Xu et al., 2015), and large-scale hydrologic models are appropriate alternatives to estimate soil moisture, evapotranspiration (ET), and runoff, which are important factors in characterizing the climate change impacts on droughts (Mishra and Singh, 2010; Kang and Sridhar, 2017; Grillakis, 2019). For instance, the Soil and Water Assessment Tool (SWAT) (Arnold et al., 1998) has been widely used to simulate historical droughts (Guo et al., 2017;), drought forecasting (Kang and Sridhar, 2021), and climate change impacts on droughts (Sam et al., 2019; Kang et al., 2021; Li and Fang, 2021) in the MRB. In addition, the Variable Infiltration Capacity (VIC) model (Liang et al., 1994) was also used in the MRB for real-time drought monitoring (Zhang et al., 2020), impacts of drought on rice productivity (Abhishek et al., 2021), and climate change impacts on hydrology (Sridhar et al., 2019) in the MRB. Therefore, hydrologic modeling-based drought evaluations lay the groundwork for drought assessments using multiple drought indices, as well as providing insights into drought management, preparedness, and mitigation strategies. Thus, the goals of this study are to evaluate conventional and flash drought conditions over the historical period (1981–2019) and to assess the effects of climate change on drought conditions over the next 80 years (2020–2099) using two future climate projection periods (f1: 2020–2059, f2: 2060–2099). For climate change simulations, four Coupled Model Intercomparison Project Phase 5 (CMIP5) climate models and two Representative Concentration Pathways (RCPs) were implemented. This study provides climate change impacts on droughts using multiple hydrologic models (SWAT and VIC), high-resolution meteorological dataset, and soil moisture-based drought index, and the results can serve as a guideline for water resources and drought mitigation strategies for alleviating drought concerns in the face of natural and human-induced changes in the MRB.

2. Methods

2.1. Study area

The Mekong River is a transboundary river in Southeast Asia that flows 4800 km from the Tibetan plateau to the South China Sea. The MRB is divided geographically into upper and lower regions, with the dividing point at Chiang Saen Station (Fig. 1). The MRB includes Cambodia, China, Lao PDR, Myanmar, Thailand, and Vietnam (MRC, 2005; MRC, 2010), with each country occupying 19.5%, 20.7%, 25.7%, 2.7%, 23.3%, and 8.1% of the total area (795,000 km^2), respectively (Fig. 1). In addition, the MRB occupies 88.6% of Cambodia, 89.4% of Lao PDR, 36.7% of Thailand, and 21.0% of Vietnam, demonstrating that the MRB is an important basin for many countries in Southeast Asia (MRC, 2010; Table 1). The distributions of precipitation and temperature in the basin are diverse. The annual average precipitation for each country ranges from 800 mm to 1615 mm, with the highest precipitation and average temperature ranging from 7.9 °C to 28.0 °C (Table 1) (MRC, 2005; Sheffield et al., 2006; Chen et al., 2008; Funk et al., 2015). Besides, the Lower Mekong Basin (LMB) is heavily influenced by monsoonal climate, which results in distinct wet and dry seasons; the wet season lasts from May to October, and the dry season lasts from November to April (MRC, 2005). Severe to extreme droughts have occurred in the MRB over the last few decades, and climate change is expected to exacerbate the frequency and intensity of droughts in some areas of the MRB (Thilakarathne and Sridhar, 2017; Sam et al., 2019; Li et al., 2021).

2.2. Hydrological models

The SWAT model (Arnold et al., 1998) is one of the widely used hydrological models for simulating hydrologic and water quality variables such as soil moisture, evapotranspiration (ET), runoff, sediment, nitrogen, and
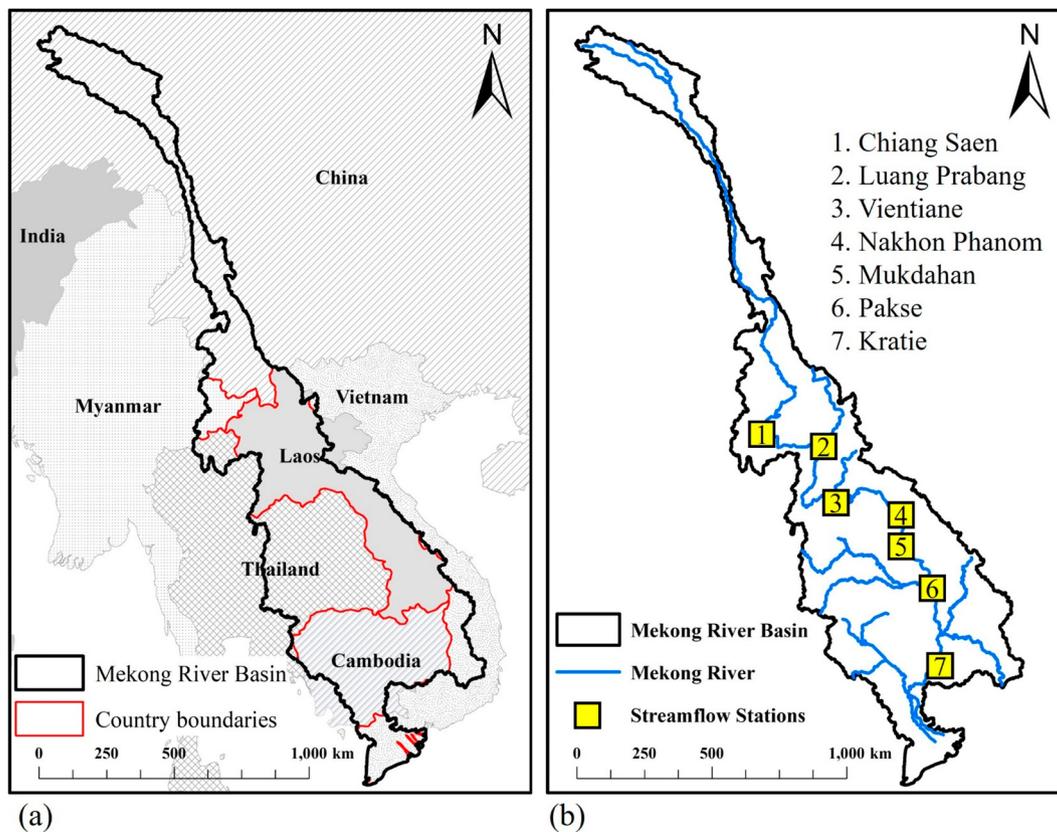
Fig. 1. Spatial maps of the Mekong River Basin (MRB). (a) Black line represents the boundary of the MRB, and red lines indicate the country boundaries. (b) Blue lines represent the Mekong River, and yellow squares indicate the streamflow stations for calibration and validation.

phosphorus, as well as the impacts of climate change (Ficklin et al., 2009; Zhang et al., 2014; Abbaspour et al., 2015; Kang and Sridhar, 2017; Kang et al., 2021). SWAT is based on hydrological response units (HRUs), which represent a specific combination of land use, soil, and slope. SWAT simulates the water budget components based on a water balance equation (Eq. (1)).

$$SW_t = SW_0 + \sum_{i=1}^{t} P_{day} - Q_{surf} - ET_a - W_{seep} - Q_{gw} \tag{1}$$

where SW_t is the final soil water (mm) on day i, t is the time (days), SW_0 is the initial soil water on day i, P_{day} is the daily precipitation (mm), Q_{surf} is the surface runoff (mm), ET_a is the evapotranspiration (ET; mm), W_{seep} is the water entering to the vadose zone from the soil layer (mm), and Q_{gw} is the return flow (mm).

Surface runoff was simulated by the modified Soil Conservation Service (SCS) Curve Number (CN) method (USDA (U.S. Department of Agriculture), 1972), which is based on daily precipitation. For the estimation of ET and potential ET (PET), the Penman-Monteith (Monteith, 1965;

Allen et al., 1998; Sridhar and Wedin, 2009; Seong et al., 2018) method was used in this study. The SWAT model requires a digital elevation model (DEM), land use, soil, and daily meteorological inputs. In this study, the Global Multi-resolution Terrain Elevation Data 2010 (GMTED2010; Danielson and Gesch, 2011) with a resolution of 250 m was used, as was the Global Land Cover Characterization (GLCC; USGS, 2021) to estimate the land use parameters, and the soil dataset was obtained from the Food and Agriculture Organization of the United Nations (Sanchez et al., 2009). For the model calibration and historical simulation, a 0.25-degree resolution of precipitation, wind speed, and temperature data from the Global Meteorological Forcing Dataset (GMFD) dataset from 1951 to 2016 (Sheffield et al., 2006) were used, while recent precipitation and temperature data (2017 to 2019 October) was generated from the Climate Hazards Group InfraRed Precipitation with Station (CHIRPS; Funk et al., 2015) and Climate Prediction Center (CPC; Chen et al., 2008) gridded dataset, respectively.

The VIC model (Liang et al., 1994) is a macroscale and semi-distributed hydrologic model that simulates water and energy balance for each grid separately, and it has been widely used to assess the hydrology and drought of many river basins around the world (Wang et al., 2011; Mao et al., 2015). In addition, the VIC model has been used in various MRB hydrological assessments (Västilä et al., 2010; Tatsumi and Yamashiki, 2015; Zhou et al., 2016; Bonnema and Hossain, 2017; Sridhar et al., 2019; Ali and Sridhar, 2019; Abhishek et al., 2021).

The vegetation characteristics represented by land cover type, leaf area index, and albedo values were generated from the Advanced Very High-Resolution Radiometer data (AVHRR; 1 km resolution). Furthermore, the soil parameters were extracted from the Harmonized World Soil Database (HWSD), which is based on the United States Department of Agriculture (USDA) classification and pedo-transfer functions (Cosby et al., 1984). The fractional value covered by each vegetation class was used to represent the contribution of different vegetation types within a grid cell. Water

Table 1
General information of six countries in the Mekong River Basin (MRB).

Countries	Occupation of the MRB (%)	Occupation for the country (%)	Annual precipitation (mm)	Annual temperature (°C)
Cambodia	19.5	88.6	1244	28.0
China	20.7	1.8	800	7.9
Lao PDR	25.7	89.4	1615	24.2
Myanmar	2.7	3.4	1210	21.9
Thailand	23.3	36.7	1239	27.3
Vietnam	8.1	21.0	1558	26.2

Table 2
Calibration parameters for the SWAT and VIC models.

Models	Parameter description	Index	Range
SWAT	Curve number for moisture condition II	r_CN2	−0.25–0.25
	Baseflow alpha factor (days)	v_ALPHA_BF	0–1
	Groundwater delay (days)	v_GW_DELAY	0–500
	Treshold depth of water in the shallow aquifer required for return flow to occur (mm)	v_GWQMN	0–1000
	Soil evaporation compensation factor	v_ESCO	0–1
	Available water capacity of the soil layer	v_SOL_AWC	0–1
	Groundwater "revap" coefficient	v_GW_REVAP	0.02–0.2
	Surface runoff lag time	v_SURLAG	0.05–24
VIC	Variable infiltration curve parameter	b_{inf}	0.1–0.5
	Depth of the second and third soil layers	D	0.1–1.5
	Fraction of maximum velocity of baseflow where non-linear baseflow begins	D_s	0–0.4
	Fraction of maximum soil moisture where non-linear baseflow occurs	Ws	0.5–1.0

v_: denotes the default parameter is replaced by a given value, and r _: means the existing parameter value is multiplied by (1+ a given value).

infiltration into the soil layers is governed by the variable infiltration curve (Wood et al., 1992), which is a non-linear function of the fractional saturated area. The VIC model has three soil layers; the first two layers respond quickly to rainfall, and the bottom layer calculates baseflow using the Arno model formulation (Franchini and Pacciani, 1991). For the estimation of total ET, the VIC model uses the Penman-Monteith method (Monteith, 1965; Allen et al., 1998), and it includes the sum of evaporation from bare soil and canopy, as well as transpiration from vegetation features. The hydrologic estimation depends on the interaction of soil and vegetation within a single grid cell, as well as meteorological variables. The VIC model was implemented at 5 km spatial resolution (0.05°) of atmospheric forcing (daily precipitation, maximum and minimum temperatures, and wind speed) in this study, and it was statistically downscaled to 0.05-degree resolution using the Intersectoral Impact Model Intercomparison Project (ISI-MIP) approach (Hempel et al., 2013). For flow routing, a separate routing approach developed by Lohmann et al. (1998; 1996) was employed to calculate the volumetric discharge at multiple locations. The unit hydrograph governed the distribution of travel time within the grid cell and implicitly accounted for travel time across hill slopes and tributaries connected to the main channel (Li et al., 2012). The routing model required the following parameters: flow direction, velocity (m/s) for the river routing component, flow diffusion parameter (m²/s), fraction of the grid cell, location of the grid cell, and grid cell impulse response function. Model accuracies for both the SWAT and VIC models were evaluated through comparison of observed and simulated streamflow at seven locations (Fig. 1), and evaluation criteria included Nash and Sutcliffe efficiency coefficient (NSE) and coefficient of determination (R^2). For the SWAT model, the Sufi-2 algorithm in the SWAT calibration uncertainty program (SWAT-CUP; Abbaspour, 2007; Abbaspour, 2013) was used, and a manual calibration approach was applied for the VIC model. Table 2 presents the calibrated parameters and their ranges. Furthermore, model-driven MSDIs were compared to the self-calibrated Palmer Drought Severity Index (scPDSI; van der Schrier et al., 2013; Blunden and Arndt, 2020) to assess how well the drought index captured drought events in the MRB (Table 3).

Table 3
Drought classifications of MSDI and SSI (Hao and AghaKouchak, 2013).

MSDI, SSI, and SPEI values	Drought categories
−2.0 or below	Extreme drought
−1.50 to −1.99	Severe drought
−1.0 to −1.49	Moderate drought
−0.99 to 0.99	Near normal
1.0–1.49	Moderately wet
1.5–1.99	Very wet
2.0 and above	Extremely wet

2.3. Terrestrial water storage

The terrestrial water storage change (TWSC) was computed using hydrological simulations and compared to satellite-based data from the Gravity Recovery and Climate Experiment (GRACE). GRACE has implemented the approach for identifying water storage changes at a 1-degree spatial and 1-month temporal resolution from the Jet Propulsion Laboratory (JPL) (Swenson and Wahr, 2006). The GRACE data provided the terrestrial water storage anomaly (TWSA), which supported the calculation the TWSC. The TWSC calculation can be expressed as follows (Eq. (2)):

$$TWSC\ GRACE(\Delta t) = TWSA_{(t_i + \Delta t)} - TWSA_{(t_i)} \tag{2}$$

where $t_i + \Delta t$ and t_i are the ending and starting times, and Δt is a time step duration.

The net water balance and TWSC were commonly calculated by the accumulation of water entering the upper section of the soil columns through precipitation and the losses of water storage due to runoff and evapotranspiration, and the mass conservation equation for TWSC is as follows (Eq. 3):

$$TWSC = P - ET + R_{in} - R_{out} \tag{3}$$

where P is precipitation, ET is evapotranspiration, R_{in} is water entering from adjacent soil, and R_{out} is runoff. In this study, the SWAT and VIC models were implemented to compute runoff and evapotranspiration for the storage change estimations. The models-driven TWSC was then compared to the GRACE-based TWSC to evaluate the hydrological responses and water storage changes over a period of 14 years (2002 to 2016).

2.4. Climate models

Based on the distribution of the changes in precipitation and temperature for the future period (2020–2099) compared to historic period (1966–2005), four global circulation models (GCM) were selected as the future precipitation and temperature. GCMs from two Representative Concentration Pathways (RCPs) 4.5 and 8.5, GFDL-ESM2M, IPSL-CM5A-LR, MIROC-ESM-CHEM, and NorESM1-M, were able to capture the distribution of wet/dry and cold/hot conditions in the future, and they were applied in many hydrological assessments in the MRB (Sridhar et al., 2019; Kang et al., 2021; Sridhar et al., 2021). The meteorological discrepancies between the GCMs were bias-corrected at 0.25-degree resolution for the SWAT model using the Intersectoral Impact Model Intercomparison Project (ISI-MIP) method based the Global Meteorological Forcing Dataset (GMFD) (Hempel et al., 2013; Sheffield et al., 2006). Precipitation and temperature data were statistically downscaled at 0.05-deg spatial resolution for the VIC simulation (about 5 km).

Table 4
Calibration results for the SWAT and VIC models.

Models	Stations	Calibration			Validation		
		Period	NSE	R^2	Period	NSE	R^2
SWAT	Chiang Saen	1984–1990	0.88	0.88	1991–1996	0.90	0.92
	Luang Prabang	1984–1990	0.89	0.91	1991–1997	0.92	0.92
	Vientiane	1984–1990	0.90	0.91	1991–1996	0.92	0.94
	Nakhon Phanom	1984–1990	0.91	0.93	1991–1995	0.82	0.90
	Mukdahan	1984–1990	0.92	0.94	1991–1995	0.86	0.92
	Pakse	1984–1990	0.89	0.91	1991–1998	0.88	0.90
	Kratie	1984–1990	0.88	0.90	1991–1998	0.85	0.89
VIC	Chiang Saen	1986–1991	0.90	0.92	1992–1997	0.88	0.88
	Luang Prabang	1986–1991	0.84	0.92	1992–1997	0.80	0.89
	Vientiane	1986–1991	0.87	0.92	1992–1996	0.90	0.94
	Nakhon Phanom	1986–1991	0.92	0.93	1992–1995	0.84	0.92
	Mukdahan	1986–1991	0.90	0.93	1992–1995	0.88	0.95
	Pakse	1986–1991	0.89	0.92	1992–1998	0.89	0.94
	Kratie	1986–1991	0.89	0.90	1992–1998	0.90	0.93

2.5. Drought indices and flash drought detections

The SWAT and VIC models were implemented to simulate various hydrologic components, such as runoff, soil moisture, evapotranspiration (ET), and potential ET (PET), which were then used to calculate two drought indices. Drought assessments based on a single hydrometeorological variable are limited in their ability to investigate the overall stages of the drought conditions when compared to assessments based on multiple variables (Hao and AghaKouchak, 2013, 2014). To account for the joint behavior of two hydrometeorological variables, Hao and AghaKouchak (2013, 2014) developed a multivariate drought evaluation approach; the multivariate standardized drought index (MSDI) was computed by the joint distribution of soil moisture and precipitation. A nonparametric-based MSDI has been used in many drought studies around the world (Hao et al., 2014; Kang and Sridhar, 2017; Real-Rangel et al., 2018; Kang and Sridhar, 2019; Kang et al., 2021). The joint distribution of two variables (X and Y) is defined as Eq. (4), and the X and Y are monthly precipitation and soil moisture, respectively.

$$P(X \leq x, Y \leq y) = p \tag{4}$$

where p is the joint probability of random variables. Also, MSDI is computed as follows:

$$MSDI = \varnothing^{-1}(p) \tag{5}$$

where $\varnothing$ is the standard normal distribution.

A nonparametric multivariate drought index (MSDI) based on empirical joint probability was employed to reduce the uncertainties of fitting the parameters (Gringorten, 1963; Yue et al., 1999; Hao and AghaKouchak, 2014) and the joint distribution was calculated by Eq. (6):

$$P(x_k, y_k) = \frac{m_k - 0.44}{n + 0.12} \tag{6}$$

where m_k is the number of occurrences when the pair (x_i, y_i) is $x_i \leq x_k$ and $y_i \leq y_k$, and n is the number of observations. The obtained joint probability is converted to MSDI (Eq. (5)). Besides, a univariate form of the Gringorten formula was used for the standardized soil moisture index (SSI) (Hao and
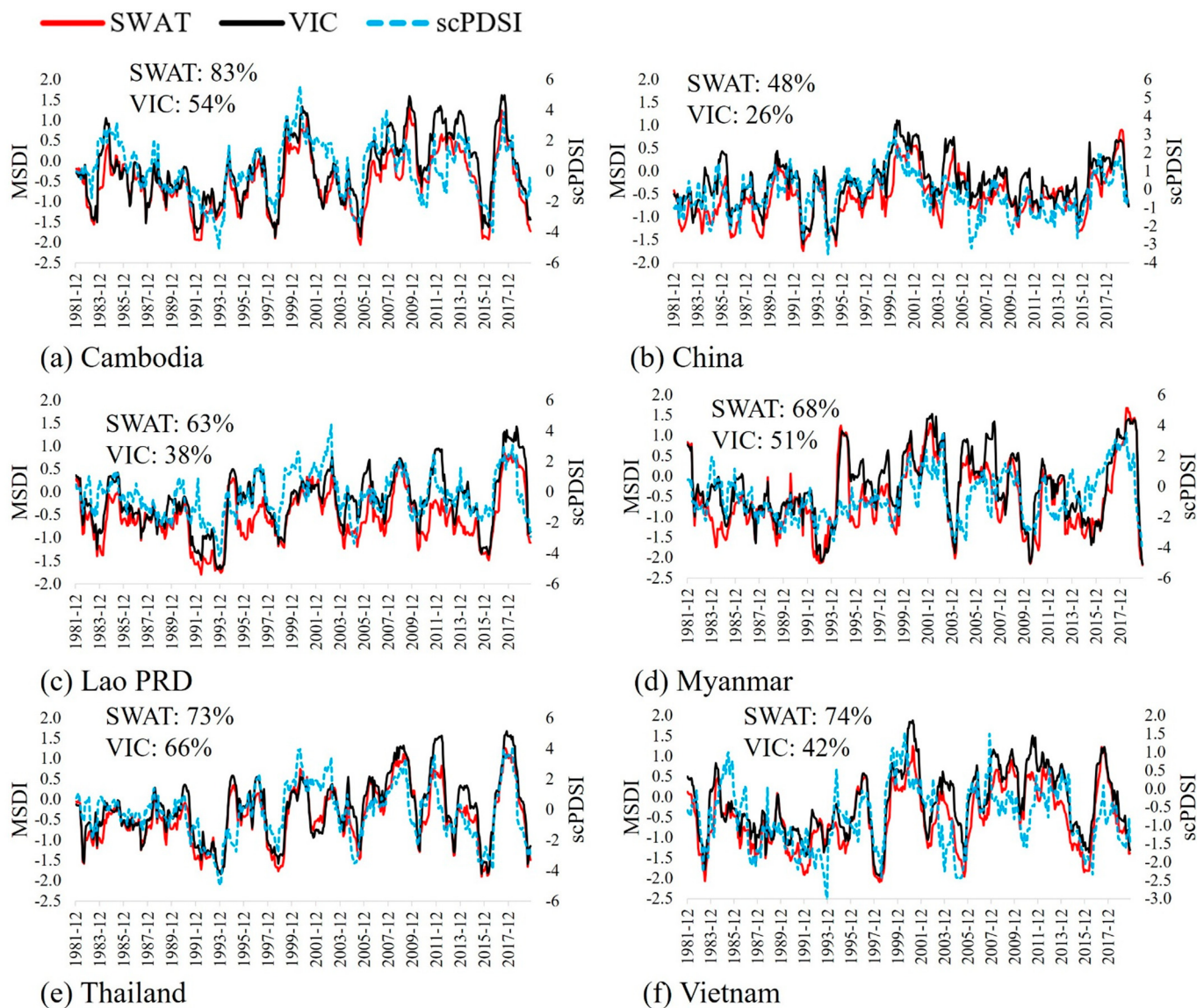

Fig. 2. Results of drought validation by a comparison of the self-calibrated Palmer Drought Severity Index (scPDSI) and Multivariate Standardized Drought Index (MSDI) from the Soil and Water Assessment Tool (SWAT) and Variable Infiltration Capacity (VIC) models. Red lines represent the time series of the SWAT-driven MSDI, black lines indicate the VIC-driven MSDI values, and blue and dashed lines are the scPDSI for each country. (a) Cambodia (b) China (c) Lao PDR (d) Myanmar (e) Thailand (f) Vietnam.
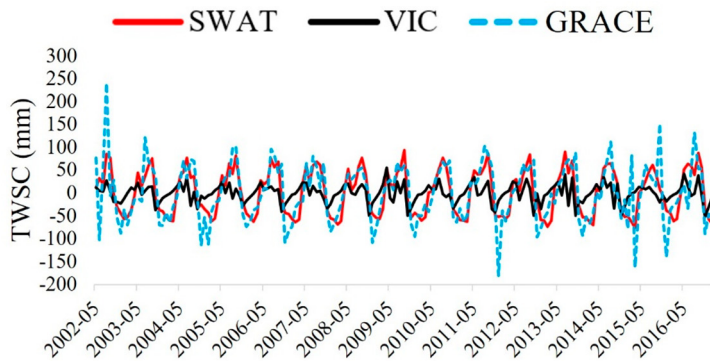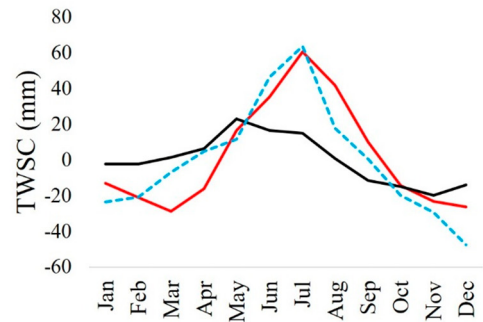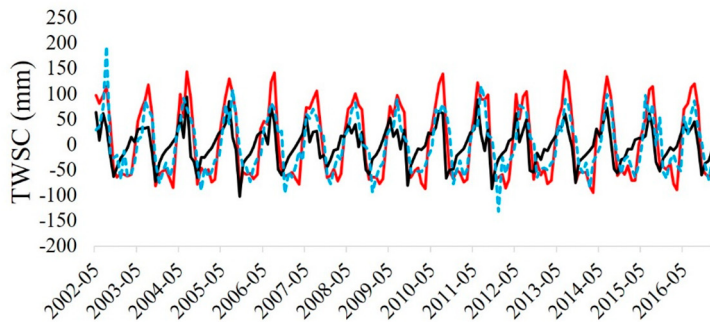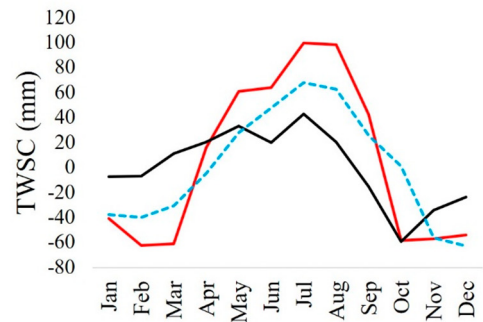
(a) Cambodia
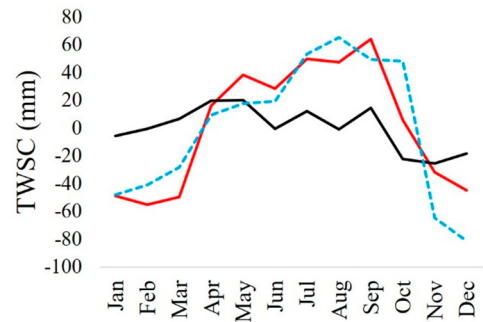
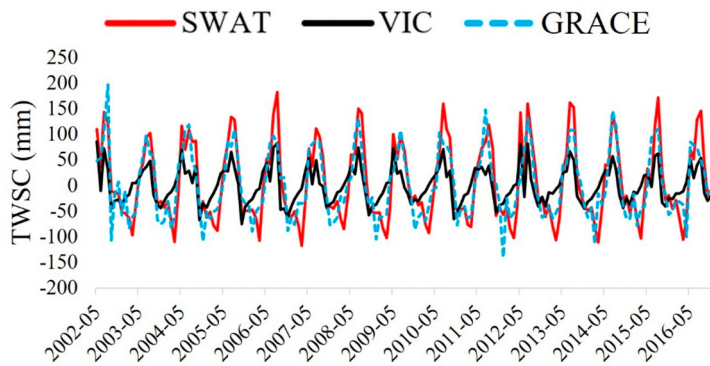(b) Cambodia – Monthly mean
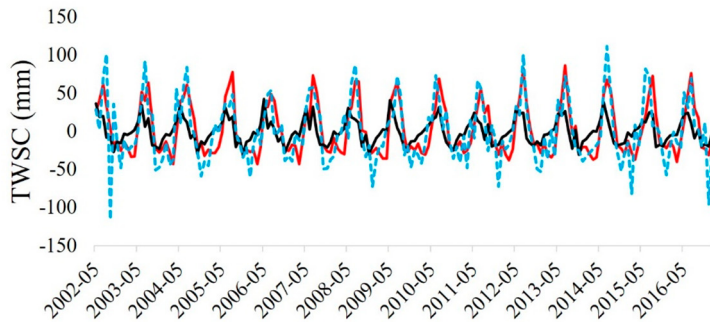
(c) China

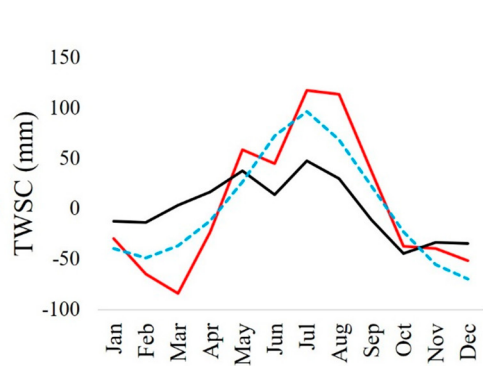(d) China – Monthly mean

(e) Lao PDR

(f) Lao PDR – Monthly mean
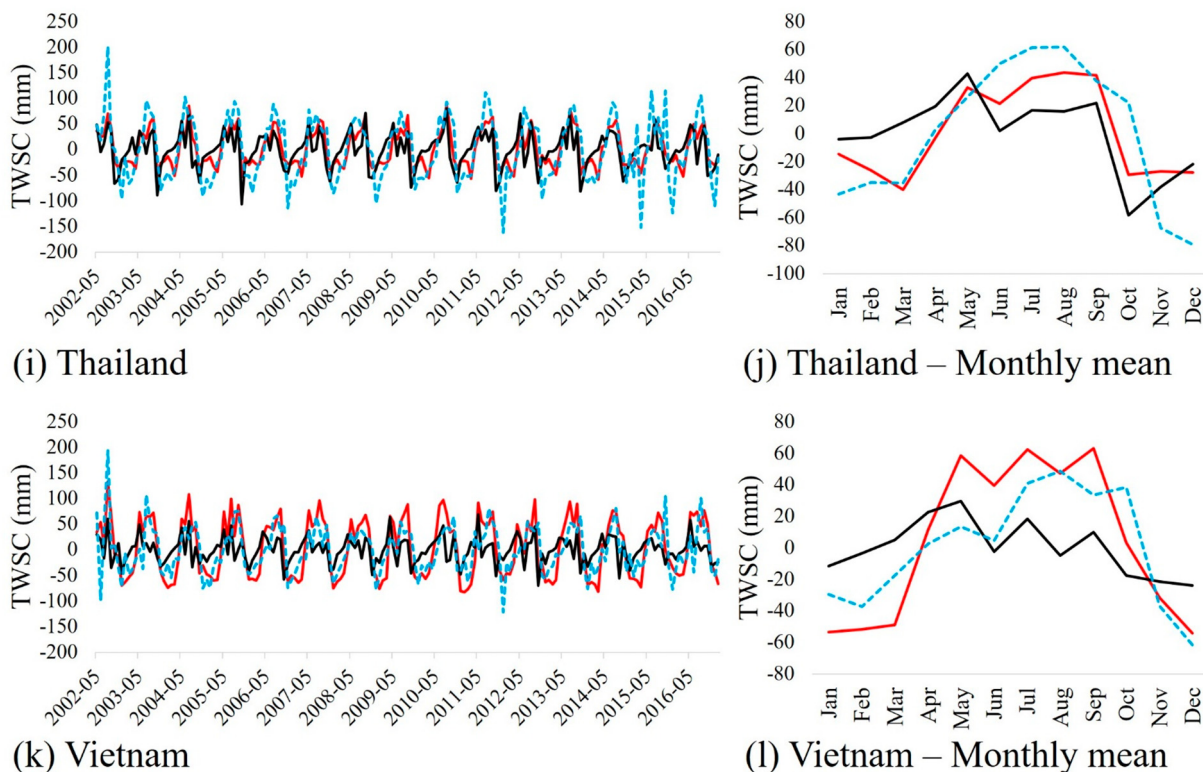
(g) Myanmar

(h) Myanmar – Monthly mean

Fig. 3. Time series and monthly average of the Terrestrial Water Storage Change (TWSC) from the hydrologic models and Gravity Recovery and Climate Experiment (GRACE). Red lines represent the time series of the SWAT-driven TWSC, black lines indicate the VIC-driven TWSC, and blue and dashed lines are the GRACE-based TWSC for each country. (a,b) Cambodia (c,d) China (e,f) Lao PDR (h,i) Myanmar (j,k) Thailand (l,m) Vietnam.

AghaKouchak, 2014) (Eq. 7). Table 2 shows the drought categories of MSDI and SSI.

$$P(x_i) = \frac{i - 0.44}{n + 0.12} \tag{7}$$

Rapid decreases in drought indices and drought persistency should be detected to identify flash droughts (Yuan et al., 2019; Parker et al., 2021), and soil moisture-based drought indices can identify the flash droughts (Ford and Labosier, 2017). In this study, the pentad (5 days) scale drought indices (i.e., MSDI and SSI) were computed to consider the rapid changes in drought conditions, and flash drought events were detected when drought indices decreased from above the 40th percentile (e.g., SSI > −0.2) to 20th percentile (e.g., SSI < −0.8) within three pentads (15 days). The flash drought events can be terminated if the drought indices return to the 20th percentile, but they should last more than three pentads (Yuan et al., 2019). The 40th percentile represents near-normal conditions, and the 20th percentile represents moderate drought conditions, according to US Drought Monitor definitions (Svoboda et al., 2002). These definitions were used in this study to assess flash drought conditions, while monthly aggregated drought indices were used to assess conventional droughts for historical and future periods.

3. Results and discussion

3.1. Model evaluation

For the SWAT models, the simulated streamflow was calibrated and validated using the SWAT-CUP, and manual calibration was carried out for the VIC model. Calibration processes were critical to guarantee that the hydrologic models' water budget simulations were accurate. Table 4 shows the calibration and validation results for the two models. For the seven observed stations in the MRB, the NSE values were greater than 0.8, which

is considered 'Very good' for the monthly simulation (Moriasi et al., 2007; Moriasi et al., 2015).

Long-term historical drought events (December 1981 to October 2019) were also verified by comparisons of scPDSI and model-driven MSDI at a moderate drought category level (scPDSI < −2, MSDI < −1). Fig. 2 presents the time series of scPDSI and MSDIs from SWAT and VIC, as well as the average calculated for each country. In Cambodia, 59 months were affected by moderate to extreme drought (scPDSI < −2) accounting for an average of 13.0% of the total period (455 months). For the other countries, Myanmar was affected by the longest period (85 months, 18.7%), China by the shortest (27 months, 5.9%), and Thailand, Cambodia, Lao PDR, and Vietnam by 70, 59, 40, and 31 months, respectively. The SWAT-driven MSDI captured 48% to 83% of the drought events during the historical observation period (1981 - October 2019), while the VIC-driven MSDI correctly estimated 26% to 66% of the drought conditions. The low level of agreement was caused by the fact that the spatial resolution of scPDSI (0.5° resolution) was different from the spatial resolutions of SWAT subwatersheds (0.25° resolution) and VIC grids (0.05° resolution). Besides, different meteorological data sources were used for these assessments. For the MSDI estimation, CHIRPS (Funk et al., 2015) and CPC (Chen et al., 2008) gridded datasets were used, but scPDSI used the Climatic Research Unit gridded Time Series dataset (CRU TS; Harris et al., 2020), which has a 15% difference in precipitation for the MRB from 1981 to 2019 (Fig. S1 in the supplementary material).

Fig. 3 presents the time series and monthly average of GRACE and model-driven TWSCs calculated by Eqs. (2) and (3), while Figs. 3(a) to Fig. 3(l) illustrate the time series and monthly average of TWSCs for each country. Red lines represent the SWAT-driven TWSC, black lines indicate the VIC-driven TWSC, and blue and dashed lines are the GRACE-based TWSC. Overall, the GRACE-based TWSC detected wet (May to October) and dry (November to April) trends, and it was clear that the SWAT-driven TWSC closely followed the overall trends for the entire countries, with seasonal variations of the SWAT-driven TWSC higher than the VIC-
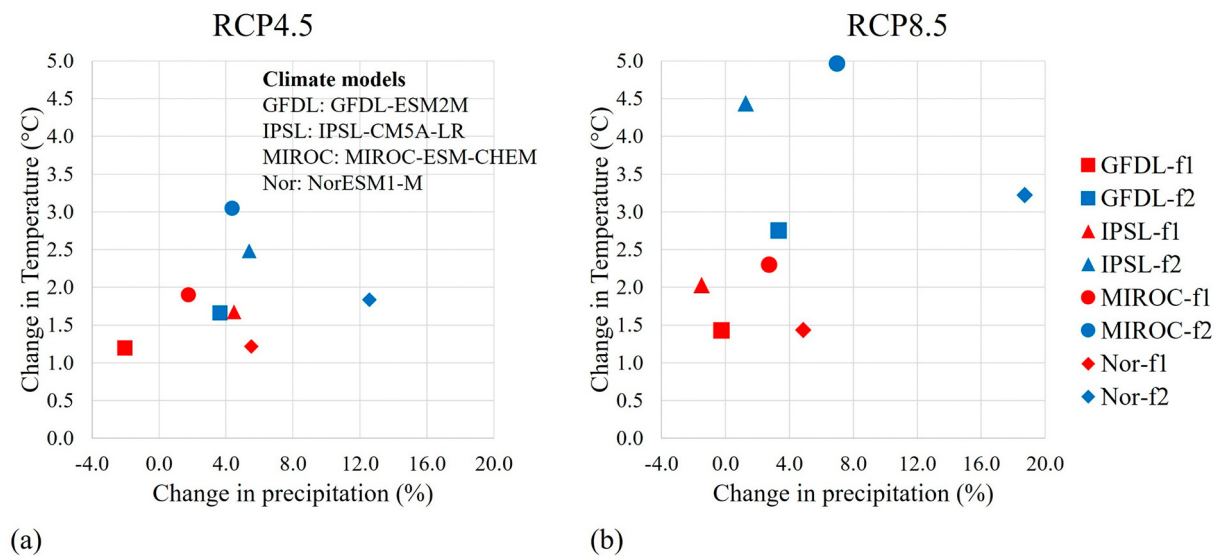
Fig. 4. Precipitation and temperature change in the MRB. The X-axis is the change in precipitation (%), and the Y-axis is the change in temperature (°C). All of the dots indicate the change in precipitation and temperature for each climate model and future periods. The red dots represent the f1 period, and the blue dots indicate the f2 period. (a) Results of RCP 4.5. (b) Results of RCP 8.5.

driven TWSC. Compared to the GRACE-based TWSC, the SWAT-driven TWSC estimated drier conditions in February, March, August, and October, and wetter conditions in May, November, and December in Cambodia. In Lao PDR, Myanmar, and Vietnam, the SWAT-driven TWSC showed drier conditions in February, March, and October, and wetter conditions from May to September. Lower seasonal variations of TWSC were observed for the VIC-driven TWSC than for the SWAT-driven TWSC, with wetter conditions were estimated from November to May and drier conditions estimated from June to October compared to the GRACE-based TWSC. Overall, both time series and monthly average, the SWAT model showed better performances for simulating the wet and dry conditions than the VIC model. This is driven by the different methodologies for water budget estimation. The hydrologic model-based water budget simulation and drought assessment is highly affected by the runoff estimation, and the two models are based on different concepts. The SWAT model uses the soil conservation service (SCS) curve number (CN) (USDA (U.S. Department of Agriculture), 1972), and the VIC model is based on the variable infiltration curve (Wood et al., 1992). The SCS CN method has been known that it has a higher sensitivity for runoff estimation (Boughton, 1989), and this could lead to those differences. The better performances were also found from the SWAT model for capturing those hydrological extremes than the VIC model (Kang and Sridhar, 2018; Sridhar et al., 2019). However, significant temporal differences were found from the model-driven TWSC. The SWAT and VIC models simulated natural flow conditions, whereas the GRACE-based TWSC included various anthropogenic activities such as dam constructions and irrigation in the MRB. In addition, the spatial resolution of the models-driven TWSC was 0.25° and 0.05°, while the GRACE-based TWSC had a resolution of 1°.
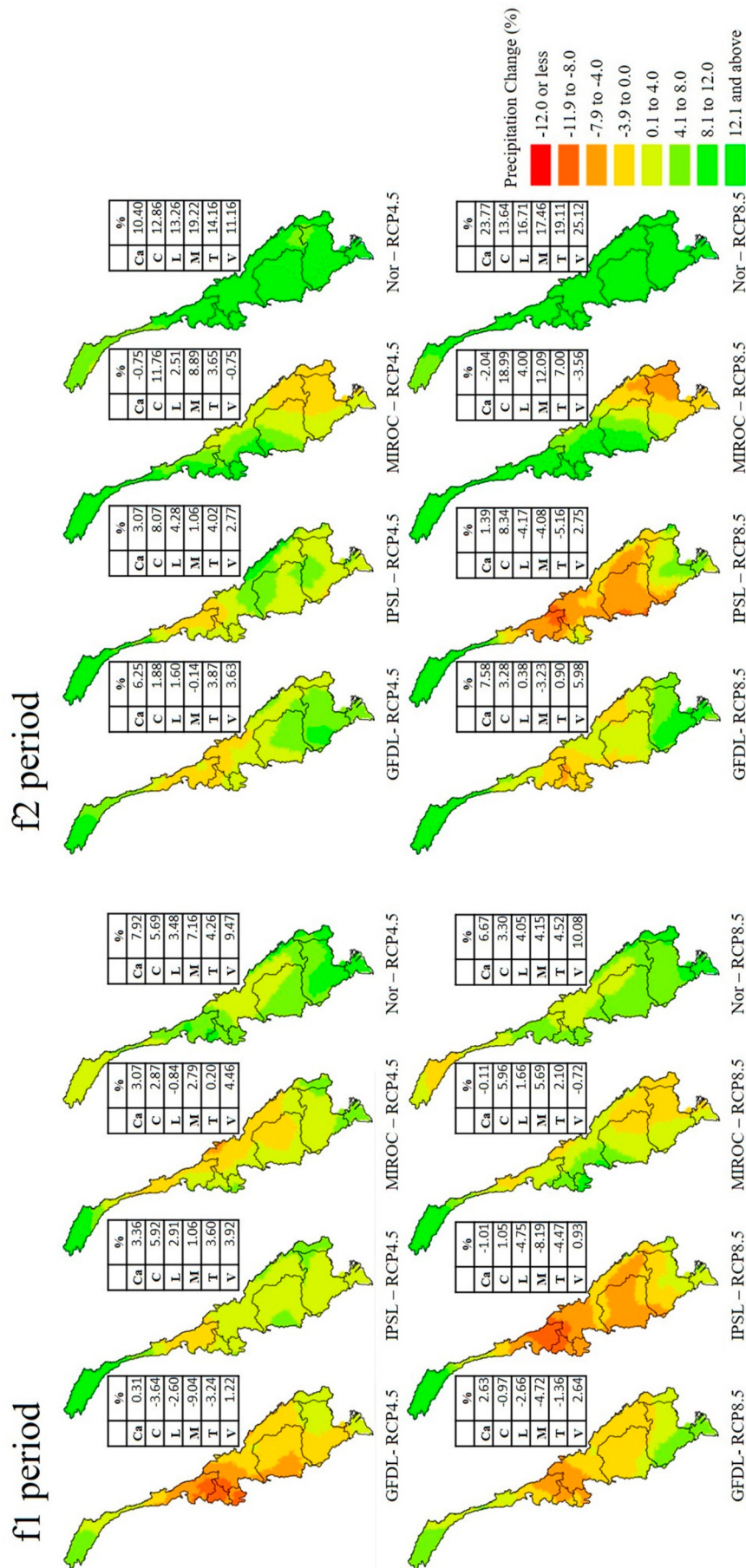
3.2. Precipitation and temperature changes

Four GCMs showed a wide range of precipitation and temperature changes, as predicted by climate models and future periods (f1 period: 2020–2059, f2 period: 2060–2099), ranging from 1.18 °C to 4.96 °C, and -2.39% and 18.71%, respectively (Fig. 4). RCP8.5 results typically showed more significant precipitation and temperature changes than RCP 4.5 results, and it is clear that the overall pattern of precipitation and temperature increases, but heterogeneous patterns may impact drought conditions in the future. The hottest scenario was found in MIROC-ESM-CHEM - RCP8.5 and f2 period (4.96 °C), the wettest in NorESM1-M-RCP8.5 and f2 period (18.7% increase), and the driest in GFDL-ESM2M-RCP4.5 and f1

period (2.27% decrease). Fig. 5 presents spatial maps of precipitation and temperature changes for each country, and the tables accompanying the figures present the changes in precipitation and temperature for each country. The wettest scenario (NorESM1-M-RCP8.5 and f2 period) resulted in the greatest increase in precipitation in Cambodia (25.12%) and Vietnam (25.12%), while the driest scenario resulted in the highest decrease in Myanmar (−9.04%). On the other hand, the IPSL-CM5A-LR-RCP8.5 scenario showed higher precipitation decreases in Lao PDR, Myanmar, and Thailand in both f1 and f2 periods (−8.19% to −4.08%), while the GFDL-ESM2M-RCP4.5 and f1 period scenario presented the highest precipitation decrease in Myanmar (−9.04%). Furthermore, the hottest scenario resulted in the highest temperature increase (6.0 °C) in China (MIROC-ESM-CHEM - RCP8.5 and f2 period).

3.3. Climate change impacts on conventional droughts

The SWAT and VIC models estimated the monthly drought indices based on simulated soil moisture for the historical and future periods (1966–2099). Fig. 6 shows the spatial patterns of drought differences between the historical and future periods, as computed by subtracting the future average of drought indices from the historical average (future drought indices – historical drought indices). The yellow to red areas (negative values) represent overall drought increases in future drought severities, whereas the green areas (positive values) indicate drought decreases. Fig. 6(a) and (b) present the results of SSI and MSDI, respectively. The SWAT-driven SSI results clearly showed overall increases in drought conditions, and the higher severities in the future were derived from a combination of precipitation decreases and temperature increases. For example, IPSL-CM5A-LR-RCP8.5 had the lowest values (−1.67 to −1.06) due to higher levels of precipitation declines (−8.19% to −4.08%) and temperature increases in Lao PDR, Myanmar, and Thailand (4.1 °C to 4.6 °C). Similarly, precipitation decreases and temperature increases were observed in the IPSL-CM5A-LR-RCP8.5 and f1 period (−1.07 to −0.66) and GFDL-ESM2M-RCP4.5 and f1 period (−0.72 to 0.06). Specifically, higher temperature increases resulted in more severe drought conditions under the same level of precipitation changes. For example, there were similar levels of precipitation increases in Cambodia (3.07%) and China (2.87%) from MIROC-ESM-CHEM – RCP4.5 and f1 period, but higher temperature increase was found in China (2.4 °C) than Cambodia (1.9 °C), resulting in more severe drought in China (−0.81) than Cambodia (−0.31) for the future period. Furthermore, severe drought increases were observed with a considerable temperature increase, as well as

Fig. 5. Spatial maps of the precipitation and temperature changes for each climate model and period. (a) Precipitation changes. Yellow to red represent decreases in precipitation, while light green to green indicate increases. The tables present the changes in precipitation for each country (%). Ca: Cambodia, C: China, L: Lao PDR, M: Myanmar, T: Thailand, V: Vietnam. (b) Temperature changes. Yellow to red indicate increases in temperature. The tables present the changes in precipitation for each country (°C).
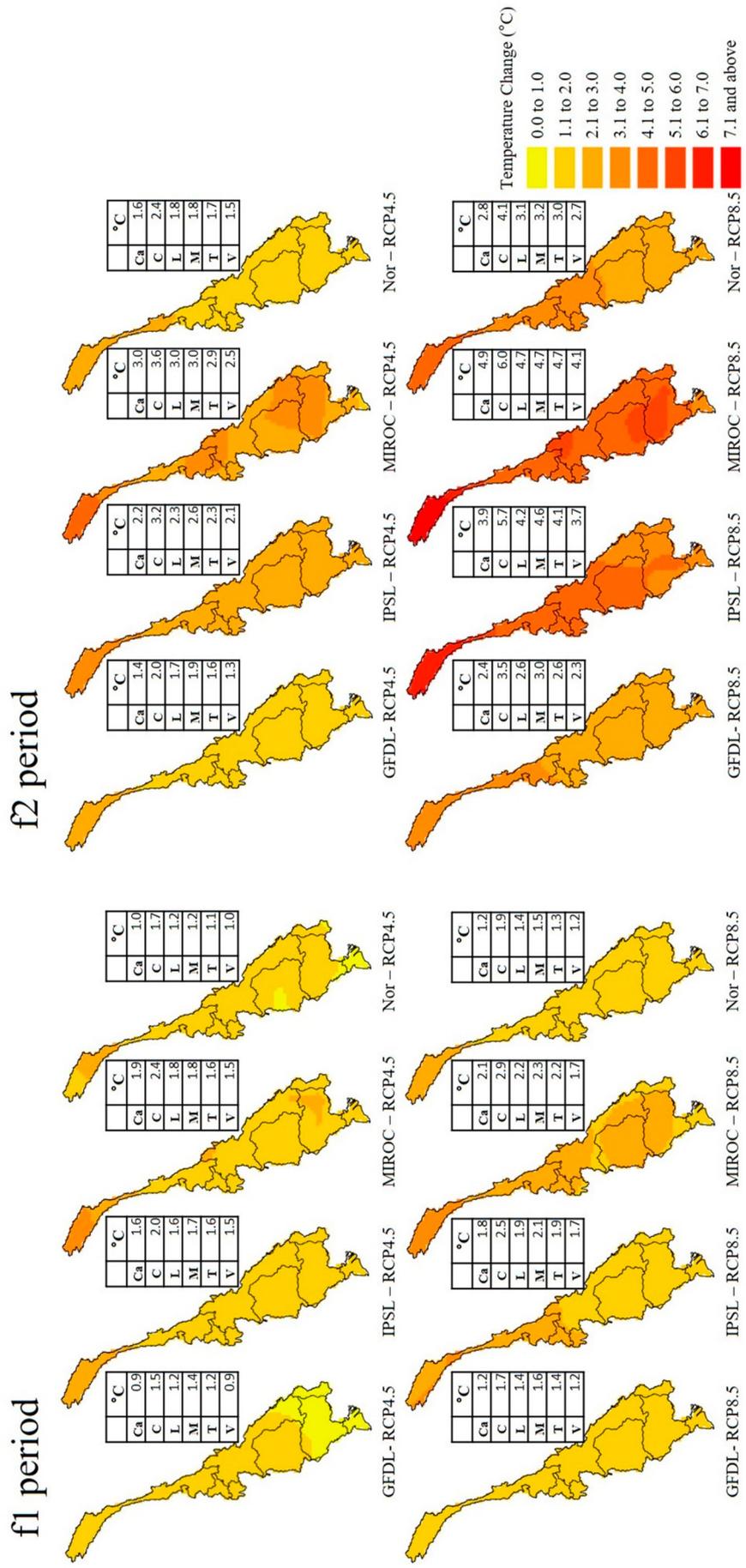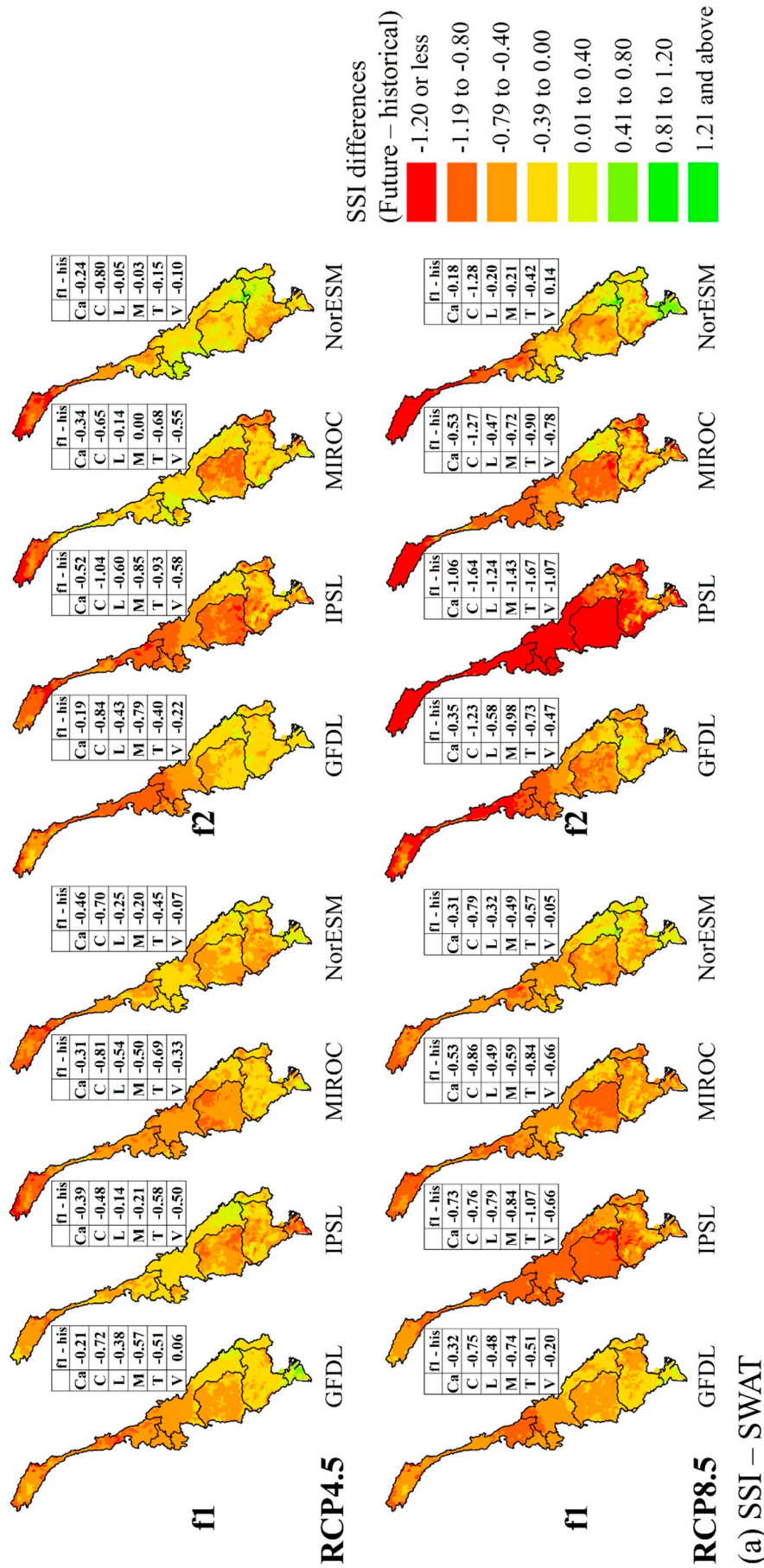
Fig. 5 (*continued*).

Fig. 6. Spatial maps of the drought differences between the historical and future periods from the SWAT model. For each sub-watershed, drought changes were computed by subtracting the future average of drought indices from the historical average (future − historical). The negative values represent the overall drought increases in drought severities during the future periods (yellow to red areas), while the positive values indicate the drought decreases (green areas). (a) SSI results (b) MSDI results.
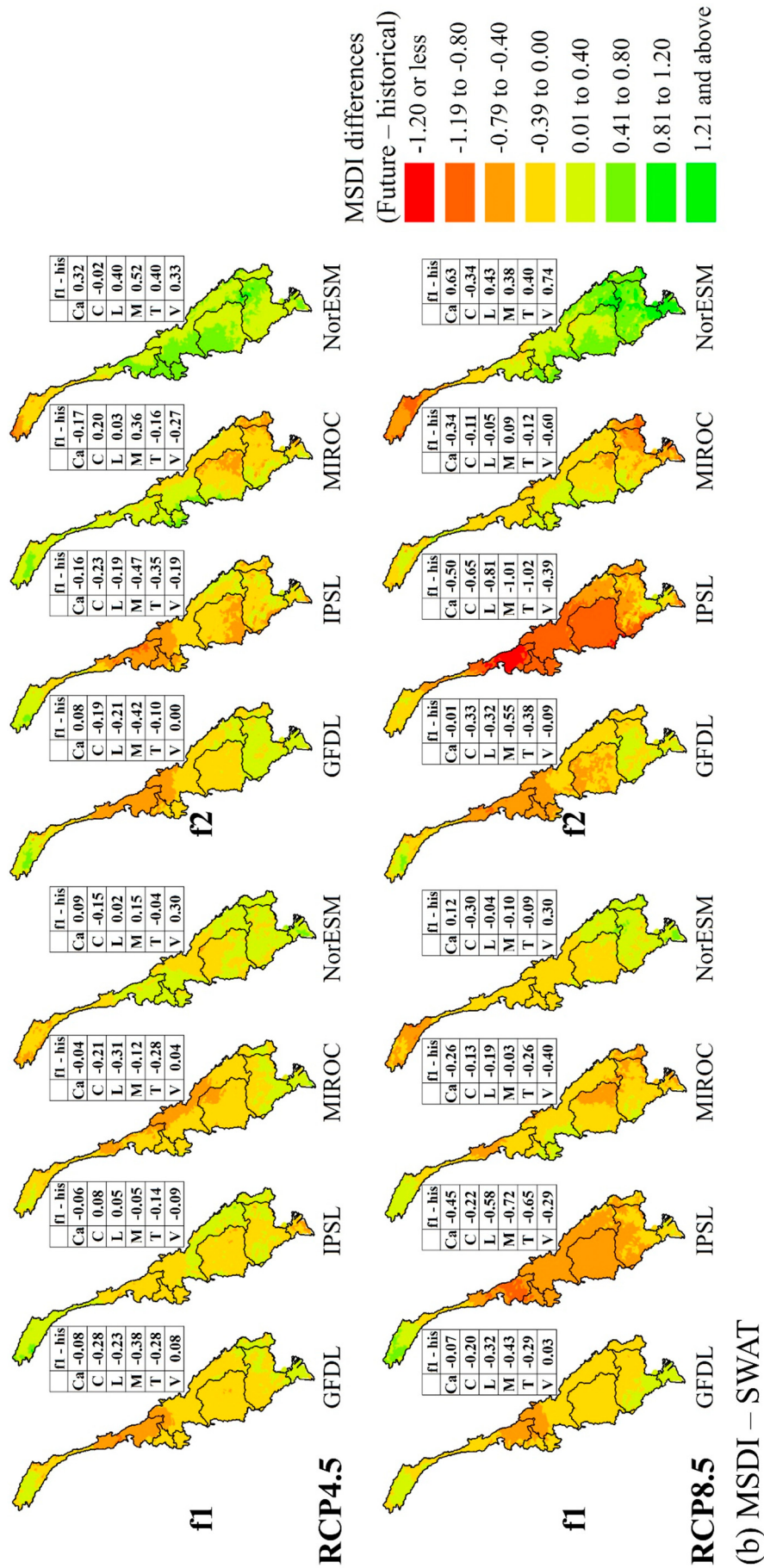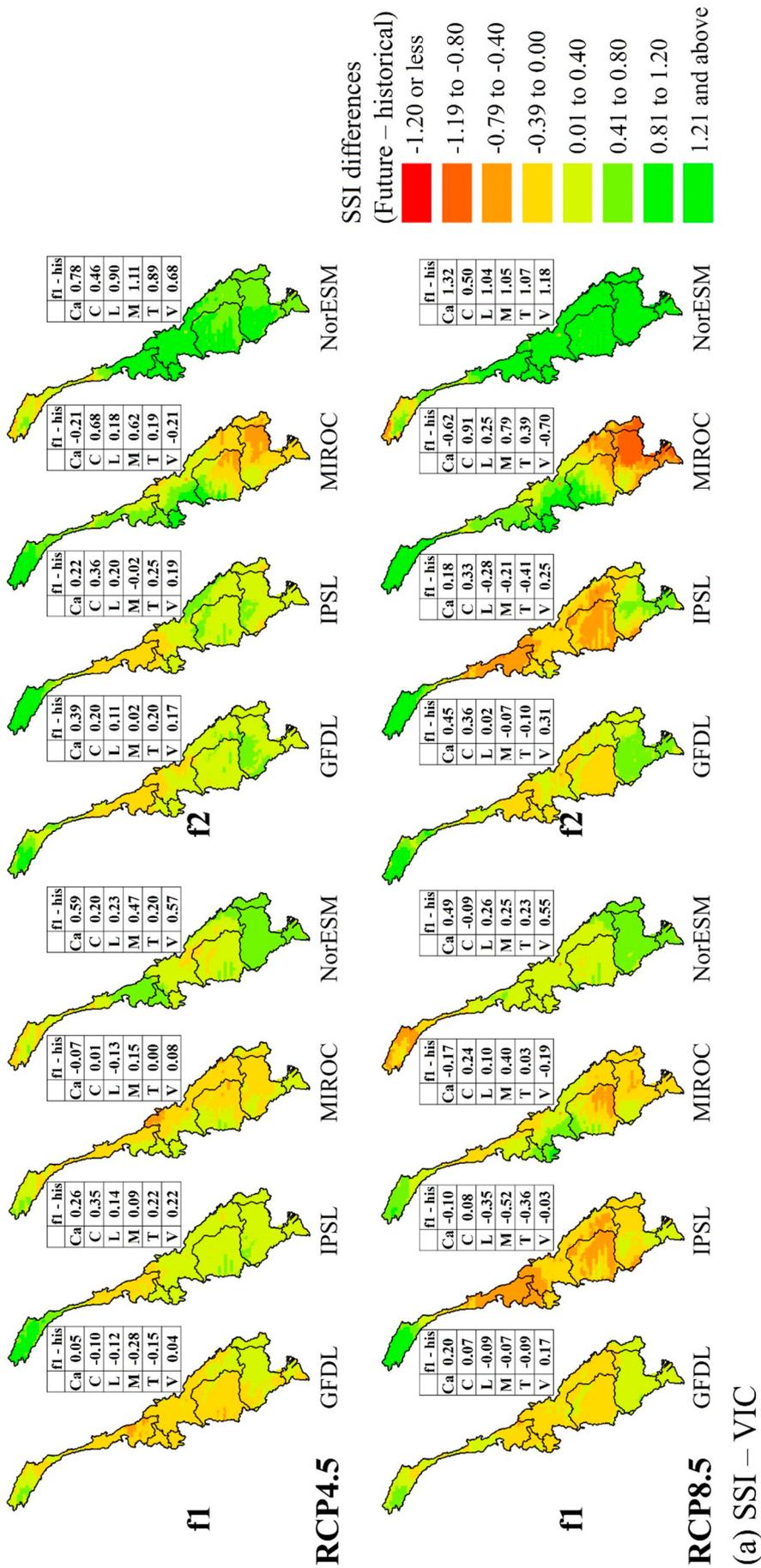
Fig. 6 (*continued*).

Fig. 7. Spatial maps of the drought differences between the historical and future periods from the VIC model. For each grid, drought changes were computed by subtracting the future average of drought indices from the historical average (future − historical). The negative values represent the overall drought increases in drought severities during the future periods (yellow to red areas), while the positive values indicate the drought decreases (green areas). (a) SSI results (b) MSDI results.
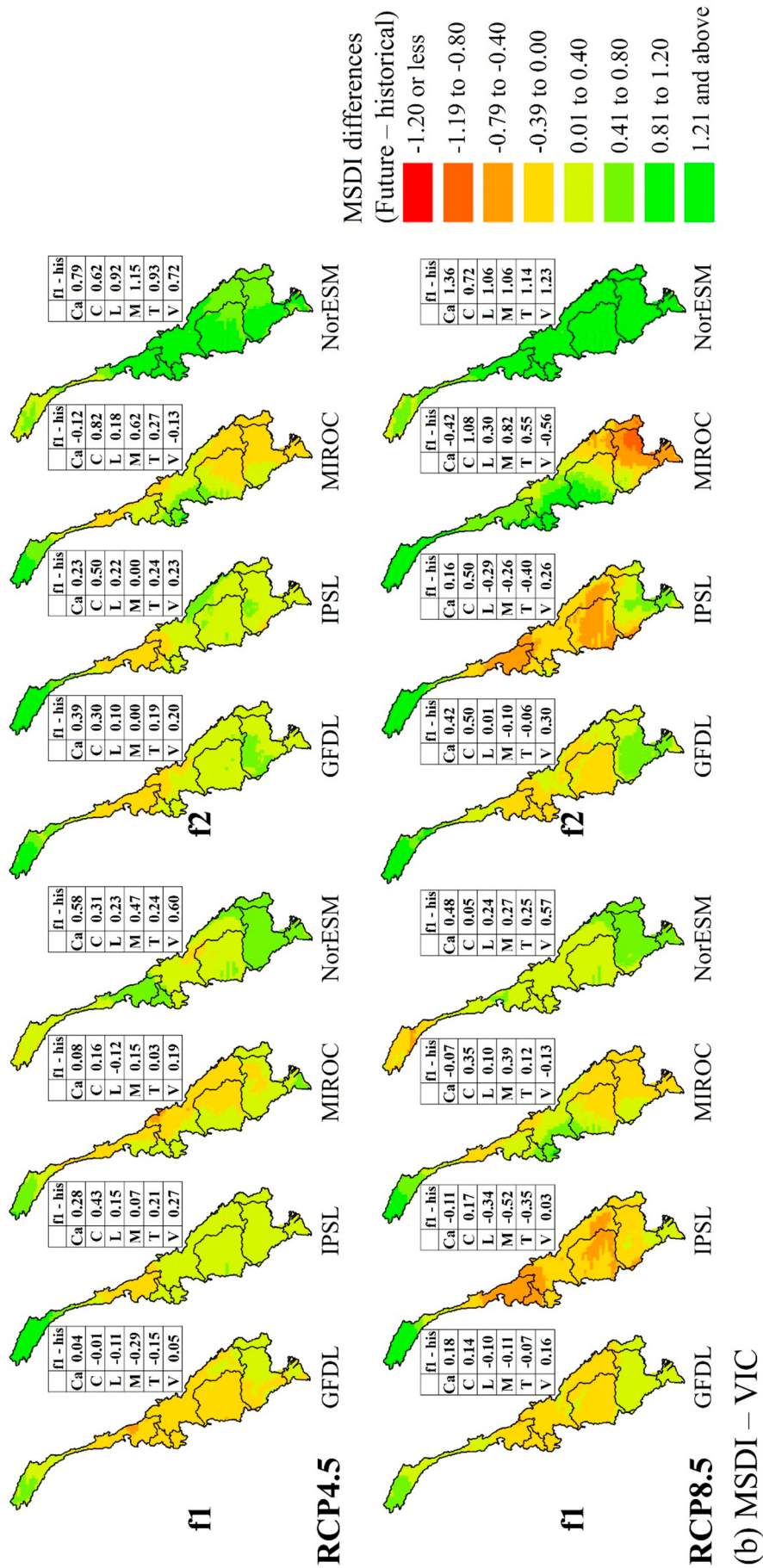
Fig. 7 (*continued*).

a substantial precipitation increase. For MIROC-ESM-CHEM - RCP8.5 and f2 period, the highest temperate increase (6.00 °C) offset 19% of the precipitation increase in China resulting in severe drought conditions in the future (−1.27). Hence, these results indicated that severe droughts in the future periods were closely related to spatial variations in hot and dry conditions, which resulted in increases in ET and declines in soil moisture (Kang and Sridhar, 2017).

Fig. 6(b) presents spatial maps of MSDI differences from the SWAT model using the same calculations as SSI. Droughts increased overall for the entire climate model and future periods, similar to the SSI results. However, the magnitudes of drought increases were smaller than the SSI because the MSDI estimation was heavily influenced by precipitation increases. From the wet climate models and periods, relatively small differences were found when compared to the SSI differences. In Thailand, for example, the NorESM1-M-RCP4.5 and f2 periods resulted in a 19.11% increase in precipitation. The difference in MSDI was 0.40, but the difference in SSI was −0.42. Furthermore, a 2.63% increase in precipitation was observed in Cambodia from the GFDL-ESM2M-RCP 4.5 and f2 periods, with MSDI and SSI differences of −0.07 and − 0.32, respectively.

The behavior of VIC-driven drought indices, on the other hand, was somewhat different. Figs. 7(a) and (b) show the SSI and MSDI from the VIC model, respectively. Drought conditions improved overall, but the general pattern of the changes was comparable to the SWAT-driven drought indices. The results of IPSL-CM5A-LR-RCP8.5 had negative values from most of the countries during both the f1 and f2 periods, with the SWAT-driven SSI having the lowest values. Furthermore, the majority of countries had negative values from GFDL-ESM2M-RCP4.5 and f1 period, with the lowest precipitation decrease (up to −9.04%) and temperature increase (up to +1.5 °C). The highest differences were found between NorESM1-M-RCP4.5 and f2 period (up to 1.11) and NorESM1-M-RCP8.5 and f2 period (up to 1.32), which corresponded to the SWAT-driven SSI with the highest

precipitation increases among the climate models and periods. The differences in drought conditions between historical and future periods for the VIC-driven MSDI were similar to those in SSI, but higher values were found in some regions where precipitation increases were reported. For example, the MIROC-ESM-CHEM-RCP4.5 and f2 periods resulted in an 11.76% increase in precipitation in China. The difference in SSI was 0.68, but the difference in MSDI was 0.82. Also, a 3.07% of precipitation increase was recorded for the MIROC-ESM-CHEM-RCP8.5 and f1 period. The difference in SSI was −0.07, but the difference in MSDI was 0.08. The IPSL-CM5A-LR-RCP8.5 and f2 periods resulted in a 6.25% increase in precipitation in Cambodia The difference in SSI was 0.33, but the difference in MSDI was 0.50.

3.4. Flash drought evaluation

3.4.1. Historical observation (1981 to 2019)

In this study, the flash drought occurrences were estimated using 5-days intervals (pentads) of SSI and MSDI for the historical observation period (1981 to 2019), and simulated daily soil moisture and precipitation were aggregated into a five-day average. Figs. 8 and 9 present the spatial distribution of flash droughts based on the two models and drought indices, with DJF (December, January, February), MAM (March, April, May), JJA (June, July, August), SON (September, October, November) representing each season. Overall, more flash droughts occurred during the JJA and SON periods than during the DJF and MAM periods in both the SWAT and VIC models. Fig. 10 presents the average flash drought occurrences from the two models and drought indices during the historical observation period, with 2847 pentads recorded (73 pentads for each year). The highest flash droughts occurred from VIC-MSDI, with 67, 92, 109, and 120 pentads for the DJF, MAM, JJA, and SON periods, accounting for 9.4%, 12.9%, 15.3%, and 16.9% of the total period. From SWAT-MSDI, there were 63,
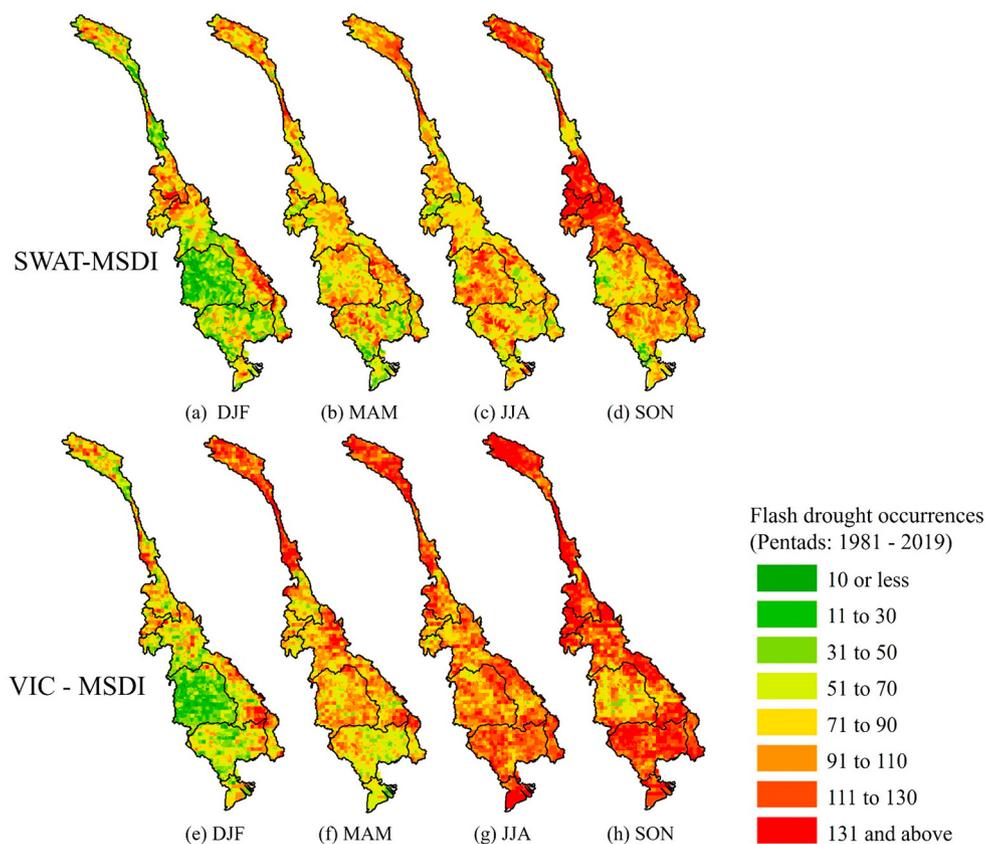

Fig. 8. Spatial maps of the flash drought occurrences during the historical observation (1981 – October 2019). (a) to (d) represent the results of SWAT-MSDI for the December to February (DJF), March to May (MAM), June to August (JJA), and September to November (SON) periods, respectively. (e) to (h) indicate the results of VIC-MSDI. Green to light green show the lower levels of the flash drought occurrences, while yellow to red represent the higher levels of flash drought occurrences.

Fig. 9. Spatial maps of the flash drought occurrences during the historical observation (1981 – October 2019). (a) to (d) represent the results of SWAT-SSI for the DJF, MAM, JJA, and SON periods, respectively. (e) to (h) indicate the results of VIC-SSI. Green to light green show the lower levels of the flash drought occurrences, while yellow to red represent the higher levels of flash drought occurrences.
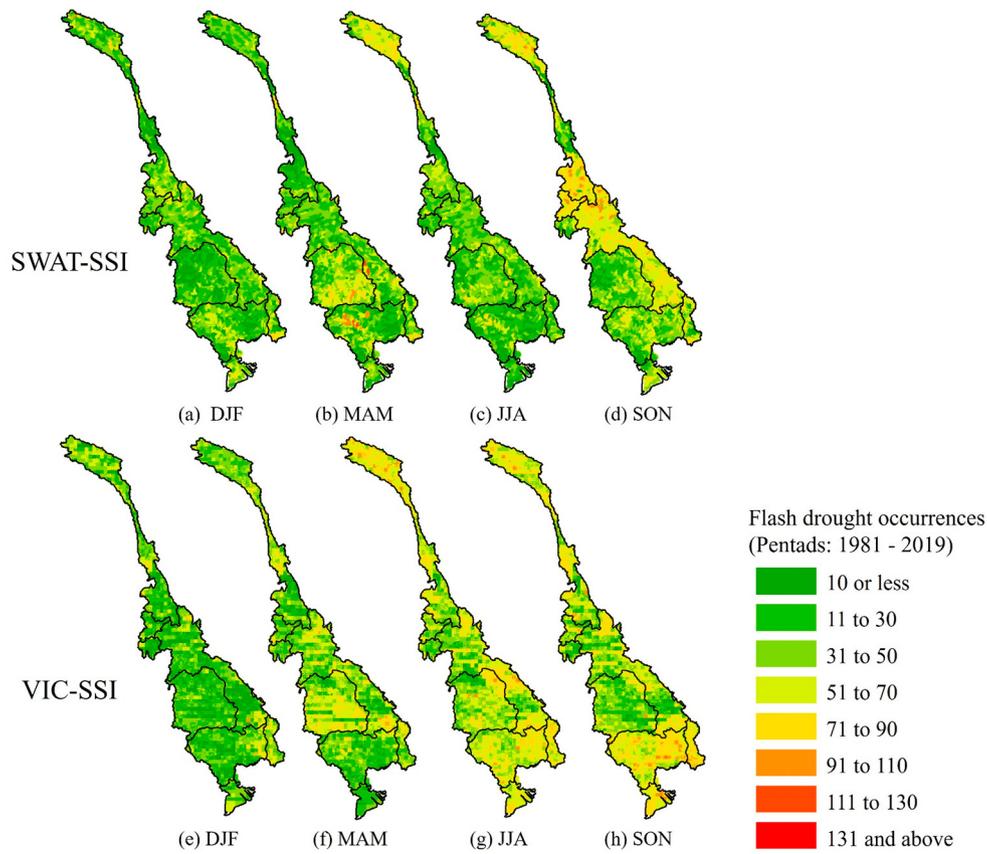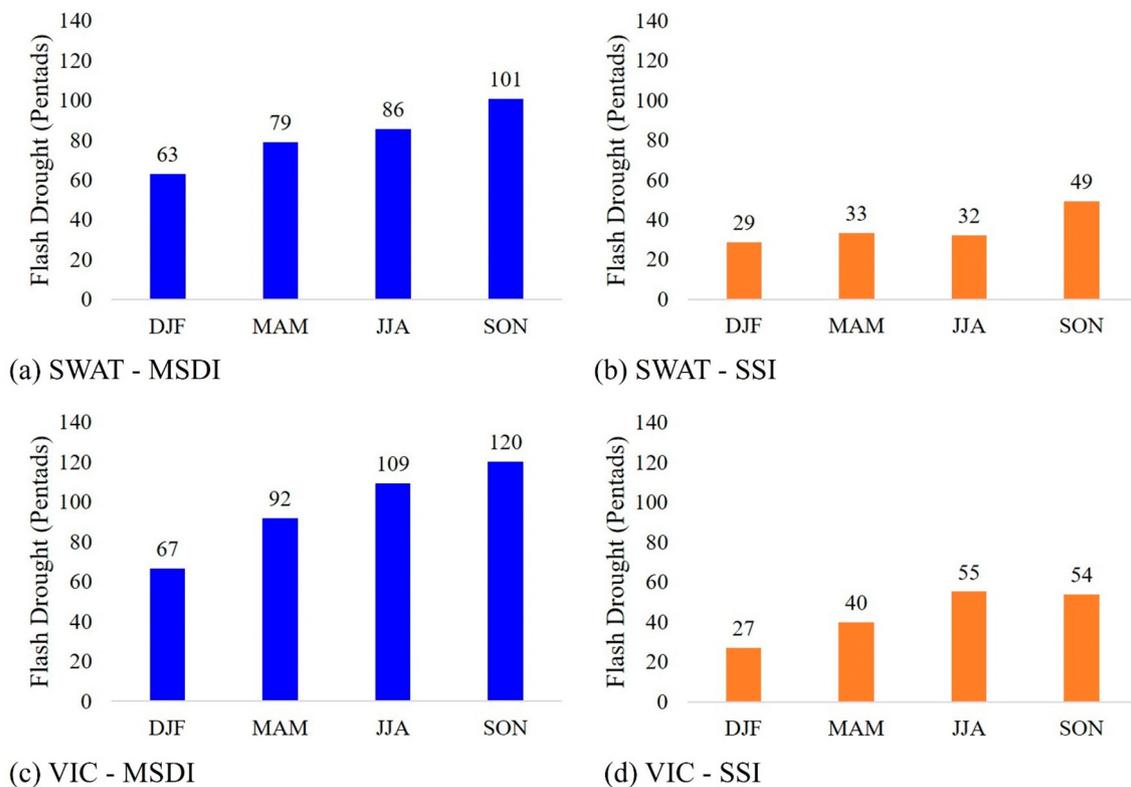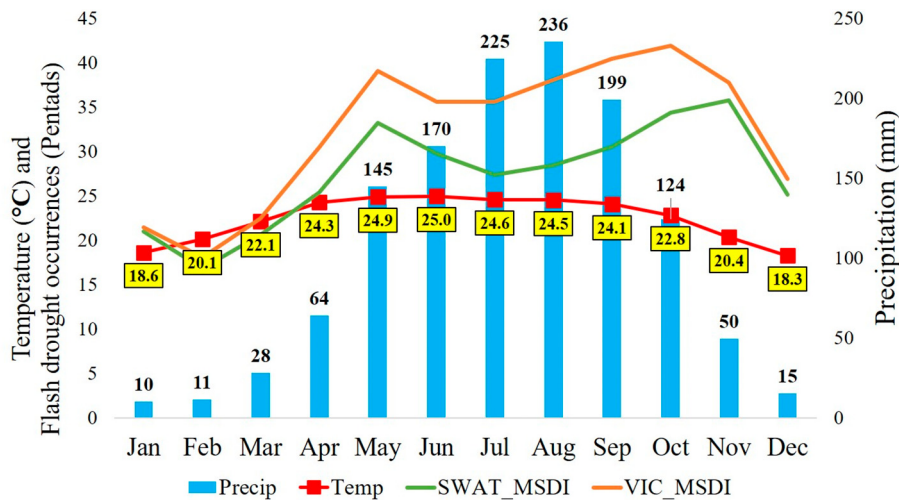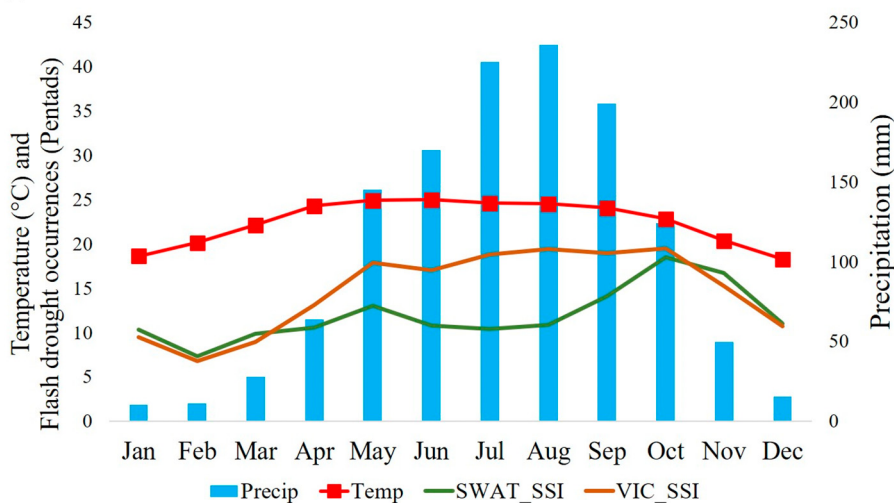

Fig. 10. Bar charts of the average flash drought occurrences during the historical observation (1981 – October 2019). (a) Results of SWAT-MSDI (b) Results of SWAT-SSI (c) Results of VIC_MSDI (d) Results of VIC – SSI.

(a) MSDI results

(b) SSI results

Fig. 11. Monthly precipitation, temperature, and flash drought occurrences of MSDI and SSI during the historical observation (1981–2019). Temperature and flash drought occurrences are represented by the primary Y axis (left), and precipitation (bar charts) is represented by the secondary Y axis (right). (a) Results of MSDI. Blue bars indicate the monthly precipitation, red line represents the monthly average temperature, green line is the flash drought occurrences from SWAT-MSDI, and brown line is the flash drought occurrences from VIC-MSDI. The black text indicates the monthly precipitation (mm), and black text with yellow boxes represent the monthly average temperature (°C). (b) Results of SSI. Dark green line is the flash drought occurrences from SWAT-SSI, and dark brown line is the flash drought occurrences from VIC-SSI.

73, 86, and 101 pentads of flash droughts Flash drought occurrences were lower in the SSI than in the MSDI. SWAT-SSI generated flash droughts of 29, 33, 32, and 49 pentads, while VIC-SSI generated flash droughts of 27, 40, 55, and 54 pentads. In general, more droughts were captured by MSDI because it monitors both precipitation and soil moisture drought conditions (Hao and AghaKouchak, 2013, 2014).

Fig. 11 shows monthly precipitation, temperature, and flash drought occurrences in the MRB, and these figures account for general flash drought behavior. The overall patterns of the SWAT and VIC models are similar, and the flash drought occurrences are highly affected by precipitation and temperature variations. In the case of MSDI, the most frequent flash droughts occurred in May, October, and November due to the higher temperatures and relatively less precipitation than during the JJA period. Precipitation (145 mm) was lower in May than in JJA, but the temperature was nearly the same or higher (24.5 °C to 25.0 °C). In October and November, precipitation started to decrease (124 mm to 50 mm), but a higher temperature level resulted in flash droughts. In the JJA period, the temperature was highest (up to 25.0 °C), but the monsoonal climate with 170 mm to 236 mm precipitation prevented the flash drought from occurring In the DJF period, relatively few flash droughts occurred due to the lower

temperature during the winter season (18.3 °C to 20.1 °C). In the case of SSI, overall patterns correspond to those of MSDI, but the occurrences of flash drought were lower than those of MSDI.

3.4.2. Climate change impacts on flash droughts

This study evaluated the impacts of climate change on flash drought occurrences in the MRB based on five-day interval drought indices from the SWAT and VIC models. The flash drought occurrences in the future period (2020–2099) were compared to the historical period (1966–2005). The future periods were divided into two parts: the near future (f1: 2020–2059) and the far future (f2: 2060–2099), with each period lasting 40 years (2090 pentads). Figs. 12 and 13 present the average occurrences of flash drought from the four climate models based on the model-driven drought indices. Fig. 12 presents the results of the SWAT model, while Fig. 13 shows the results of the VIC model.

The overall patterns of flash drought occurrences in the future periods were similar to those observed in the past. More flash droughts occurred during the JJA and SON periods than during the DJF and MAM periods due to the lower precipitation and higher temperatures, which corresponded with historical observations. The SWAT-driven MSDI and
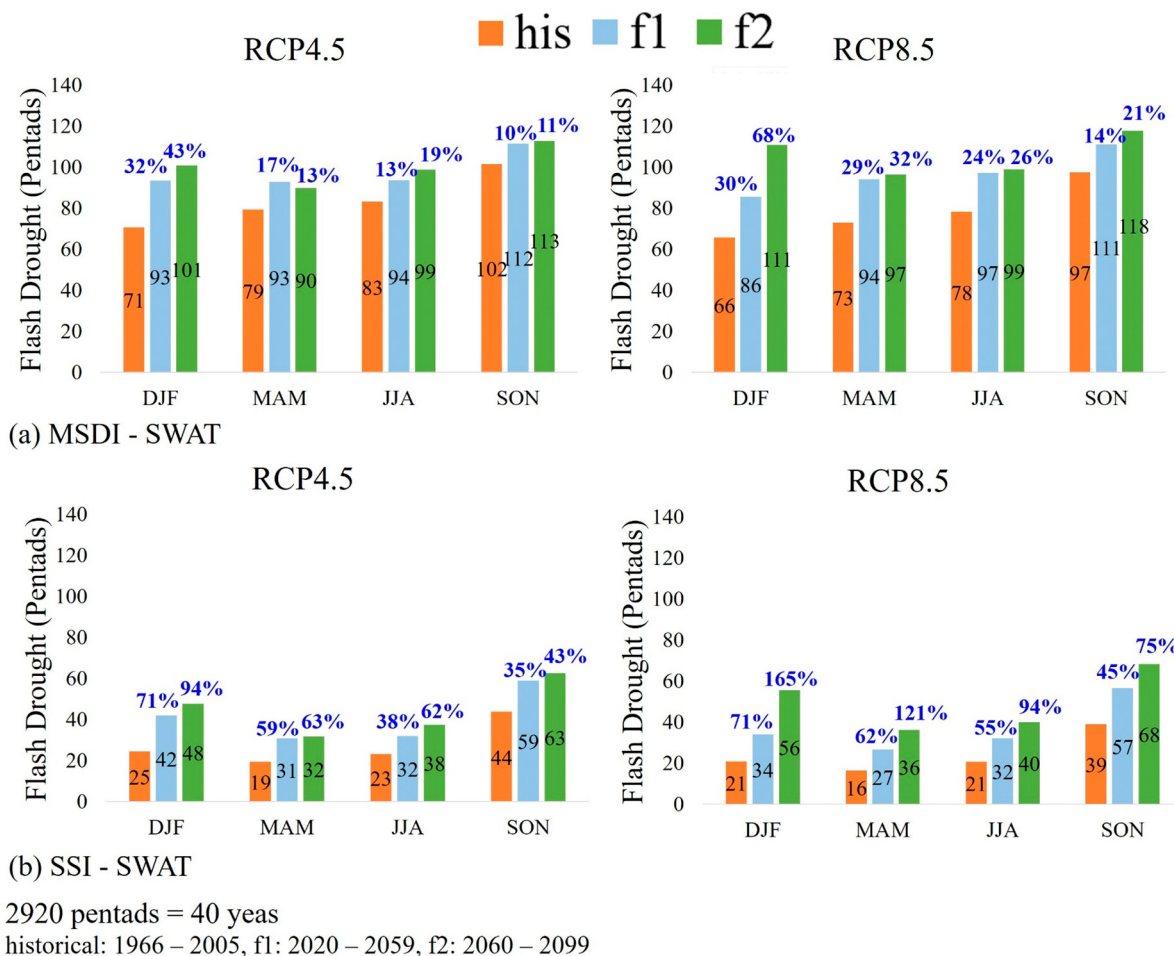
Fig. 12. Bar charts of the average flash drought changes during the future period (f1: 2020–2059, f2: 2060–2099). Light blue bars represent the results of the f1 period, and green bars indicate the results of the f2 period (a) Results of SWAT-MSDI for RCP4.5 (b) Results of SWAT-MSDI for RCP8.5 (c) Results of SWAT_SSI for RCP4.5 (d) Results of SWAT – SSI for RCP8.5.

SSI (Fig. 12) showed an increase in flash drought occurrences for all seasons and future periods, corresponding to the SWAT model's conventional drought conditions. Furthermore, future temperature increases were found for all four seasons (Fig. 14(c) and (d)), and they would have a significant impact on flash drought occurrences in the future. Compared to the f1 period, more flash droughts occurred during the f2 period, and the results of RCP8.5 produced more flash droughts than RCP4.5 due to higher temperature increases. From the results of SWAT-MSDI and RCP4.5, there were 32%, 17%, 13%, and 10% increases in flash droughts during the f1 period, and 43%, 13%, 19%, and 11% increases during the f2 period for DJF, MAM, JJA, and SON, respectively. From the SWAT-MSDI and RCP8.5, 30%, 29%, 24%, and 14% increases were found for the f1 period, and 68%, 32%, 26%, and 21% increases for the f2 period. The rates of increase for the DJF period were higher than other periods because the historical temperature during the DJF period (18.8 °C) was relatively lower than other periods (22.7 to 25.1 °C), causing flash drought conditions to react more sensitively to the higher rates of the temperature increases (7.3% to 19.1%). For the MAM period, there were increases in flash drought occurrences (13% to 32%), which was primarily due to temperature increases of 7.5% to 17.8% and precipitation decreases of −7.5% to −0.1%. The JJA and SON periods also saw an increase in flash droughts (10% to 21%), but the magnitudes of the increases were smaller than those seen in the DJF and MAM periods due to lower temperature increases (5.0% to 16.7%).

The overall flash drought occurrences captured by SWAT-SSI were lesser than MSDI (Fig. 12(b)), correlating with historical observations (Fig. 10). As with the MSDI results, more flash droughts occurred during the f1 period than the f2 period, and the results of RCP8.5 produced more flash droughts than RCP4.5, which were highly correlated with temperature and precipitation variations. From the results of SWAT-SSI and RCP4.5, there were 71%, 59%, 38%, and 35% increases in flash droughts during the f1 period, and 94%, 63%, 62%, and 43% increases in the f2 period for DJF, MAM, JJA, and SON, respectively. From RCP8.5, there were 71%, 62%, 55%, and 45% increases in the f1 period, and 165%, 121%, 94%, and 75% increases in the f2 period. In addition, the patterns of future flash drought changes resembled MSDI. The highest increases were found in the DJF period (71% to 165%), and the lowest increase rates were seen in the SON period (35% to 75%).

From the VIC-driven MSDI and SSI (Fig. 13), there were decreases in flash drought occurrences for future periods, which corresponded to the conventional drought conditions predicted by the VIC model. From the results of the VIC-MSDI and RCP4.5, there were − 3%, 6%, 3%, and − 7% increases and decreases in flash droughts during the f1 period, and − 11%, −1%, −1%, and − 12% decreases in the f2 period for DJF, MAM, JJA, and SON, respectively. From RCP8.5, there were −7%, 14%, 8%, and −6% increases and decreases in the f1 period, and − 9%, 2%, 0%, and − 10% increases and decreases for the f2 period. According to the VIC-SSI and RCP4.5 results, there were − 22%, − 3%, 6%, and 11% increases and decreases in flash droughts during the f1 period, and − 36%, − 3%, 6%, and 11% increases and decreases were found in the f2 period for DJF, MAM, JJA, and SON, respectively. From RCP8.5, there were −38%, 2%, 5%, and −13% increases and decreases in the f1 period, and −44%, −20%, −5%, and −20% increases and decreases in the f2 period.

Each GCM and future period is depicted in Figs. S2-S5 in the Supplement materials. Overall, higher magnitudes of flash drought increase
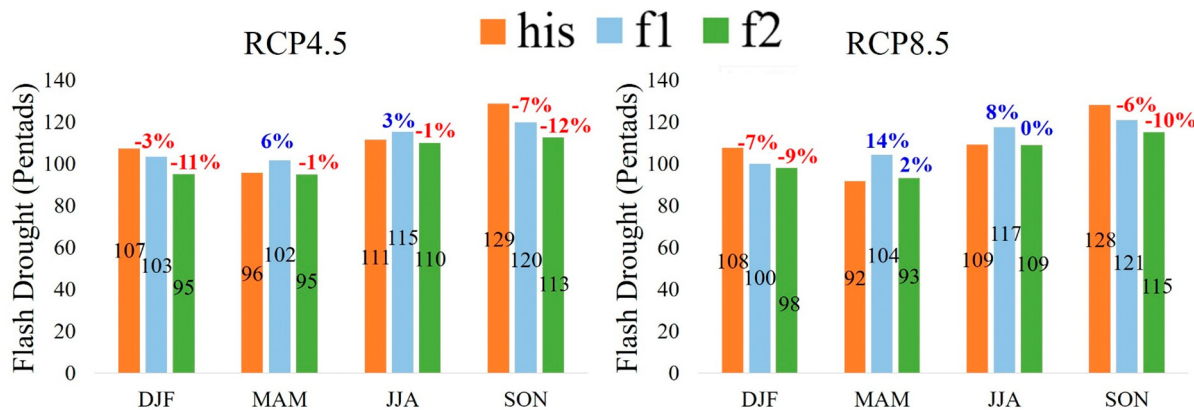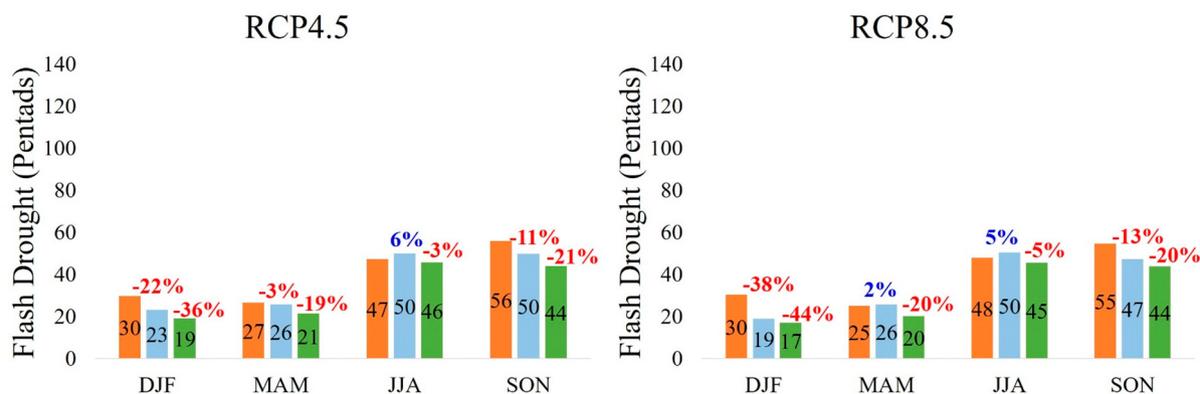
Fig. 13. Bar charts of the average flash drought changes during the future period (f1: 2020–2059, f2: 2060–2099). Light blue bars represent the results of the f1 period, and green bars indicate the results of the f2 period (a) Results of VIC-MSDI for RCP4.5 (b) Results of VIC-MSDI for RCP8.5 (c) Results of VIC_SSI for RCP4.5 (d) Results of VIC – SSI for RCP8.5.

occur in scenarios with less precipitation or a slight increase in precipitation and a higher temperature increase. However, higher precipitation increases mitigate future increases in flash drought occurrences. Fig. S2 depicts the SWAT-MSDI results, which show that there was a decrease in precipitation (− 2.0%) and a lower level of temperature increase (1.2 °C) from the GFDL-ESM2M-RCP4.5 and f1 periods, resulting in a 44% increase in flash drought in the JJA period. In addition, the IPSL-CM5A-LR-RCP8.5 and f2 periods have a higher level of temperature increase (4.4 °C), and a lower level of precipitation increase (1.3%), resulting in flash drought increases of up to 158% (30% to 158%). The MIROC-ESM-CHEM-RCP8.5 and f2 period produced the highest temperature increase (5.0 °C) but a higher precipitation increases (7.0%) mitigated the increase in flash drought in the future (31% to 52%) compared to the IPSL-CM5A-LR-RCP8.5 and f2 period. The NorESM1-M-RCP8.5 and f2 period experienced 3.2 °C temperature increases (moderate level), but the highest precipitation increase (18.7%) mitigated the flash drought increase (− 11% to 34%).

The variability of precipitation and temperature changes had a significant impact on the increase in flash drought in the case of SWAT-SSI (Fig. S3). A higher temperature increase (4.4 °C) and a lower precipitation increase (1.3%) from IPSL-CM5A-LR-RCP8.5 and f2 period resulted in 345% increase in flash drought (82% to 345%). However, the NorESM1-M-RCP4.5 and f1 period showed lower temperature increases (1.2 °C) and moderate precipitation increase (5.5%), resulting in fewer flash drought (− 2% to 81%). Also, there was a temperature increase (3.2 °C) but the highest precipitation increase (18.7%) from the NorESM1-M-

RCP8.5 and f2 period, which helped to mitigate the flash drought increase (11% to 127%).

The results of VIC-MSDI showed increases and decreases in flash droughts according to the GCMs and future periods, and they also responded sensitively to changes in precipitation and temperature (Fig. S4). The NorESM1-M-RCP8.5 and f2 period showed a moderate level of temperature increase (3.2 °C) but the highest precipitation increase (18.7%), resulting in flash drought reductions (− 35% to − 8% increases). In the case of IPSL-CM5A-LR-RCP8.5 and f2 period, a high level of temperature increase (4.4 °C) and a lower level of precipitation increase (1.3%) resulted in flash drought increases of up to 32% (− 9% to 32%). The GFDL-ESM2M-RCP8.5 and f2 period showed a 3.6% precipitation increase and a lower temperature increase (1.7 °C), resulting in increases in flash drought (4% to 14%). However, there were overall flash drought decreases (− 15% to 0%) from the GFDL-ESM2M-RCP4.5 and f2 period, which were caused by the moderate temperature increase (2.8 °C). The results of VIC-SSI showed decreases and increases in flash drought based on GCMs and future periods, and the results were similar to the VIC-MSDI results. For instance, the NorESM1-M-RCP8.5 and f2 period resulted in flash drought decreases (− 59% to − 13% increases), while the IPSL-CM5A-LR-RCP4.5 and f1 period resulted in flash drought decreases (− 33% to − 4%). In addition, overall flash drought decreases (− 32% to 3%) were projected from the GFDL-ESM2M-RCP4.5 and f2 period.

Both conventional and flash drought assessments, the SWAT model usually generated more drought events than the VIC model for the future
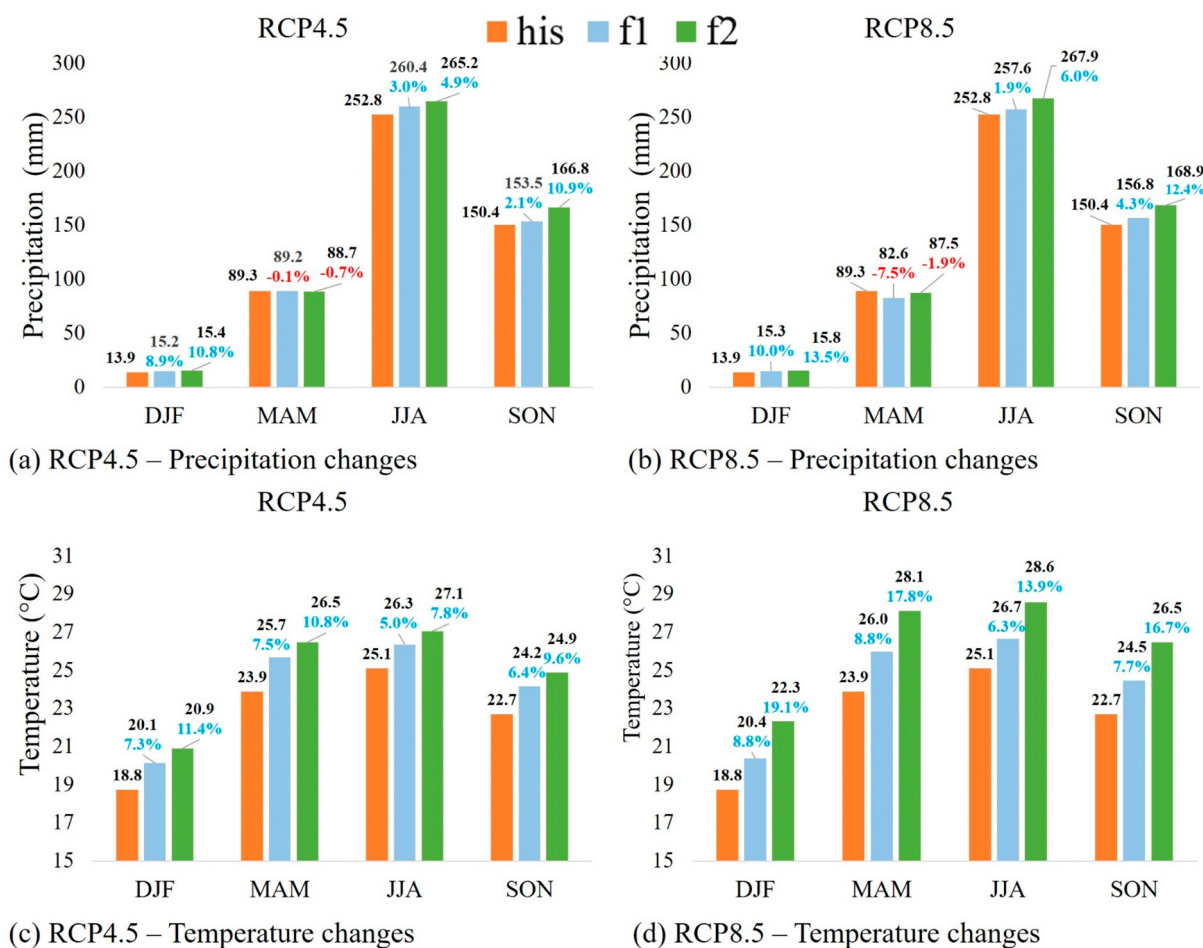
Fig. 14. Precipitation and temperature changes for each season and future periods. Orange bars indicate the average of the historical period (1966–2005), light blue and green bars represent the average of the f1 and f2 periods, respectively. Black text represents the data labels for each bar, and blue and red text indicate the increase (blue) or decrease (red) rates during the future periods. (a) Precipitation changes for RCP4.5 (b) Precipitation changes for RCP8.5 (c) Temperature changes for RCP4.5 (d) Temperature changes for RCP8.5.

period. Similar patterns were found during the historical period. For instance, the SWAT-driven MSDI produced 114 months of moderate to extreme droughts (MSDI < −1) in Cambodia, but the VIC-driven MSDI generated 80 months. The SWAT-driven MSDI produced 84, 80, 159, 91, and 131 months of drought events for other countries, but the VIC-driven MSDI generated 31, 45, 88, 76, and 69 months for China, Lao PDR, Myanmar, Thailand, and Vietnam, respectively (Fig. 2). On average, the VIC model produced only 59% of the drought events compared to the SWAT model. Similar to the TWSC estimation, different water budget estimations generated those differences, and the SWAT model captured more drought events due to its higher sensitivities, which derived different drought characteristics of conventional and flash droughts for the future period.

Drought has detrimentally affected many regions in the MRB, and the impacts of droughts have been exacerbated by climate change. In this study, for conventional and flash droughts assessments, the SWAT-driven drought indices displayed overall increases in drought conditions, while the VIC-driven showed decreases. Numerous studies have also investigated the climate change impacts on the drought characteristics in the MRB using various hydrologic and climate models, and they usually concluded that more severe and intense droughts would occur in the MRB. For example, Thilakarathne and Sridhar (2017) pointed out that more frequent and severe droughts are expected in the Lower LMB and 3S regions in the future period and predicted overall drought increases in the LMB except the Chi-Mun region in Thailand based on the multivariate drought assessment. Sam et al. (2019) assessed the climate change impacts on drought

conditions in the Srepok River Basin, and there were remarkable increases in drought severity, duration, and frequency for meteorological, hydrological, and agricultural droughts. Li et al. (2021) evaluated future meteorological and hydrological drought conditions in the MRB, and they found that the intensity of meteorological and hydrological drought will increase in the near future (2010–2039). Dong et al. (2022) focused on the seasonal characteristics of drought in the MRB based on the Sixth Phase of Coupled Model Inter-comparison Project (CMIP6) and found that a 60% increase in total drought events in the near future (2021–2055) and more than 80% increases in the far future (2061 2095). In this study, the historical drought evaluations pointed out that the SWAT-driven drought index accurately captured (48% to 83%) more than the VIC-driven drought index (26% to 66%). Therefore, based on the literature review and historical drought evaluation, it can be concluded that the SWAT-driven drought assessments are better than the VIC model for the future drought assessment in the MRB.

3.4.3. Anthropogenic perspectives of droughts

Traditional definitions of drought depict a deficit or abnormality in water-related variables such as soil moisture, groundwater storage, precipitation, runoff, evaporative demand, and snowpack, and drought is generally regarded as a product, not a process under these definitions (AghaKouchak et al., 2021). Droughts, on the other hand, should be defined and demonstrated as a complex dynamic of both natural and human-made alterations and their dynamic interactions. In this study, the direct human-induced changes such as dam constructions, land-use change, agricultural expansion, and growth of water demands driven by population increase

were not included in the drought analyses. However, precipitation and temperature changes caused by various human activities in the future were considered to evaluate the impact of climate change on conventional and flash drought conditions in the Mekong River basin using various climatic scenarios, two hydrologic models, four climate models, and two RCPs that consider a wide range of precipitation and temperature changes. RCP4.5 is an intermediate scenario that stabilizes radiative forcing at 4.5 W/m^2 in the year 2010 (Moss et al., 2008; Thomson et al., 2011), and RCP8.5 is designed by an additional 8.5 W/m^2 radiative forcing that is commonly represented by the most aggressive and extreme fossil fuel use (Schwalm et al., 2020). The average precipitation increases of RCP4.5 were 2.4% and 6.5%, and RCP8.5 were 1.5% and 7.6% for the f1 and f2 periods, respectively. In addition, the average temperature increases of RCP4.5 were 1.5 °C and 2.3 °C, and RCP8.5 were 1.8 °C and 3.8 °C, indicating that the RCP8.5 results predicted more extreme climatic conditions in the future. These patterns were also evident in the results of conventional and flash drought conditions. For example, in the results of SWAT-MSDI flash drought changes, there were 10% - 43% increases from RCP4.5, and 14% - 68% increases from RCP8.5. In the case of SWAT-SSI, there were 35% - 94% increases from RCP4.5 and 45% - 165% increases from RCP8.5 (Fig. 12). These findings clearly demonstrated that greater anthropogenic changes (i.e., RCP8.5) resulted in more extreme and uncertain climatic and drought conditions in the future.

The MRB is a transboundary river basin with numerous inter-country relations and human-induced changes. Recent dam constructions in upstream regions have altered streamflow variability, posing a threat to downstream livelihoods and economies (Soukhaphon et al., 2021), and these changes have exacerbated the recent destructive droughts (Lu et al., 2021). Thus, the combined effects of current climate change and human-induced changes should be considered concurrently, which can investigate the complicated dynamics of anthropogenic and natural changes and their effects on drought, and is ultimately useful for drought mitigation plans, water resource management, and MRB policymaking.

4. Conclusion

This study investigated future climate change impacts on conventional and flash droughts in the MRB using hydrologic simulations from the SWAT and VIC models and multiple climate change scenarios. The models were calibrated and validated by comparing simulated and observed streamflow at multiple stations, and simulated soil moisture was used to compute drought indices for historical (1966–2005) and future periods (f1: 2020–2059, f2: 2060–2099). The following are the key findings:

1. The SWAT model was calibrated and validated by comparing observed and simulated streamflow with SWAT-CUP, whereas the VIC model was calibrated by manual parameter adjustments. Drought conditions were also validated by comparing the estimated drought index (MSDI) from the two models and scPDSI over a historical observation period (1981 – Oct 2019), and the model-driven drought index reasonably reflects drought conditions across the MRB. The total drought durations by scPDSI for China, Thailand, Cambodia, Lao PDR, and Vietnam were 27, 70, 59, 40, and 31 months, representing 5.9%, 15.0%, 12.7%, 8.6%, 6.7% of the period, respectively.
2. For conventional drought conditions, monthly-scale drought indices (MSDI and SSI) were estimated for historical (1966–2005) and future periods (f1: 2020–2059, f2: 2060–2099) based on simulated soil moisture from the SWAT and VIC models. The SWAT-driven SSI and MSDI clearly showed overall increases in drought conditions in the future periods, with precipitation decrease and temperature increases being the primary drivers. However, the behaviors of VIC-driven drought indices were somewhat different, and overall drought decreases were found due to different soil moisture estimation methodologies.
3. Estimated soil moisture from the two models as well as pentad-scale (five days) MSDI and SSI during the historical and future periods, were used to investigate flash drought conditions. Because of seasonal

temperature and precipitation variations, more flash drought occurred during the JJA and SON periods than during the DJF and MAM periods. For future periods, the SWAT-driven drought indices showed overall increases in flash drought occurrences (up to 165%), while the VIC-driven drought indices showed decreases in flash drought occurrences (up to −44%). The performances of two models are significantly difference due to the different methods for water budget estimations.
4. The evaluation of climate change impacts on drought conditions in a large river basin can be assessed using multiple hydrologic models, drought indices, climate projections, and various emission scenarios, allowing for assessments of various scales of drought conditions in the future, such as conventional (monthly scale) and flash drought occurrences (pentad scale), and providing a comprehensive understanding of the future drought conditions, which could be useful for water resource management and drought mitigation strategies.
5. This is the first attempt to evaluate the historical and climate change impacts on flash drought conditions in the MRB using probabilistic-based drought indices, two hydrological models, high-resolution meteorological inputs, and a variety of climate scenarios that cover a wide range of future climatic conditions. Furthermore, as a result of the seasonal flash drought analyses, it is clear that basin countries have differential impacts, so targeted future adaptation strategy is required. In the future, to validate these findings more robust drought assessments are needed in this complex basin that take into account both natural and human-induced changes (e.g., dam impacts).

Declaration of competing interest

The authors declare that they have no known competing financial interests or personal relationships that could have appeared to influence the work reported in this paper.

CRediT authorship contribution statement

HK and VS designed the study. HK conducted SWAT simulations. SAA performed the VIC modeling analysis. VS validated the results. VS supervised the project. HK and VS and wrote the original manuscript and VS performed additional editorial checks.

Appendix A. Supplementary data

Supplementary data to this article can be found online at https://doi.org/10.1016/j.scitotenv.2022.155845.

References

Abbaspour, K.C., 2007. User Manual for SWAT-CUP, SWAT Calibration and Uncertainty Analysis Programs. Swiss Federal Institute of Aquatic Science and Technology, Eawag, Duebendorf, Switzerland, p. 93.
Abbaspour, K.C., 2013. Swat-cup 2012. SWAT Calibration and Uncertainty Program—A User Manual.
Abbaspour, K.C., Rouholahnejad, E., Vaghefi, S., Srinivasan, R., Yang, H., Kløve, B., 2015. A continental-scale hydrology and water quality model for Europe: calibration and uncertainty of a high-resolution large-scale SWAT model. J. Hydrol. 524, 733–752.
Abhishek, A., Das, N.N., Ines, A.V., Andreadis, K.M., Jayasinghe, S., Granger, S., Ellenburg, W.L., Dutta, R., Quyen, N.H., Markert, A.M., Mishra, V., 2021. Evaluating the impacts

of drought on rice productivity over Cambodia in the lower Mekong Basin. J. Hydrol. 599, 126291.

AghaKouchak, A., Mirchi, A., Madani, K., Di Baldassarre, G., Nazemi, A., Alborzi, A., Anjileli, H., Azarderakhsh, M., Chiang, F., Hassanzadeh, E., Huning, L.S., 2021. Anthropogenic Drought: Definition, Challenges, and Opportunities.

Ahmadalipour, A., Moradkhani, H., Castelletti, A., Magliocca, N., 2019. Future drought risk in Africa: integrating vulnerability, climate change, and population growth. Sci. Total Environ. 662, 672–686.

Ali, S.A., Sridhar, V., 2019. Deriving the dam characteristics from remote sensing to assess the cascading effect of dams in the Mekong River Basin. Remote Sens. 11, 2872. https://doi.org/10.3390/rs11232872.

Allen, R.G., Pereira, L.S., Raes, D., Smith, M., 1998. Crop Evapotranspiration-Guidelines for Computing Crop Water Requirements-FAO Irrigation and Drainage Paper 56. (9)300. FAO, Rome p.D05109.

Anderson, M.C., Norman, J.M., Mecikalski, J.R., Otkin, J.A., Kustas, W.P., 2007. A climatological study of evapotranspiration and moisture stress across the continental United States based on thermal remote sensing: 1. Model formulation. J. Geophys. Res. Atmos. 112 (D10).

Anderson, M.C., Hain, C., Otkin, J., Zhan, X., Mo, K., Svoboda, M., Wardlow, B., Pimstein, A., 2013. An intercomparison of drought indicators based on thermal remote sensing and NLDAS-2 simulations with US drought monitor classifications. J. Hydrometeorol. 14 (4), 1035–1056.

Arnold, J.G., Srinivasan, R., Muttiah, R.S., Williams, J.R., 1998. Large area hydrologic modeling and assessment part I: model development 1. J. Am. Water Resour. Assoc. 34 (1), 73–89.

Basara, J.B., Christian, J.I., Wakefield, R.A., Otkin, J.A., Hunt, E.H., Brown, D.P., 2019. The evolution, propagation, and spread of flash drought in the Central United States during 2012. Environ. Res. Lett. 14 (8), 084025.

State of the climate in 2019. In: Blunden, J., Arndt, D.S. (Eds.), Bull. Am. Meteorol. Soc. 101 (8), S1–S429.

Bonnema, M., Hossain, F., 2017. Inferring reservoir operating patterns across the Mekong Basin using only space observations. Water Resour. Res. 53 (5), 3791–3810.

Boughton, W.C., 1989. A review of the USDA SCS curve number method. Soil Res. 27 (3), 511–523.

Cheeseman, J., 2016. Food security in the face of salinity, drought, climate change, and population growth. Halophytes for Food Security in Dry Lands. Academic Press, pp. 111–123.

Chen, M., Shi, W., Xie, P., Silva, V.B., Kousky, V.E., Wayne Higgins, R., Janowiak, J.E., 2008. Assessing objective techniques for gauge-based analyses of global daily precipitation. J. Geophys. Res. Atmos. 113 (D4).

Christian, J.I., Basara, J.B., Otkin, J.A., Hunt, E.D., Wakefield, R.A., Flanagan, P.X., Xiao, X., 2019. A methodology for flash drought identification: application of flash drought frequency across the United States. J. Hydrometeorol. 20 (5), 833–846.

Christian, J.I., Basara, J.B., Hunt, E.D., Otkin, J.A., Xiao, X., 2020. Flash drought development and cascading impacts associated with the 2010 Russian heatwave. Environ. Res. Lett. 15 (9), 094078.

Cosby, B.J., Hornberger, G.M., Clapp, R.B., Ginn, T., 1984. A statistical exploration of the relationships of soil moisture characteristics to the physical properties of soils. Water Resour. Res. 20 (6), 682–690.

Danielson, J.J., Gesch, D.B., 2011. Global Multi-resolution Terrain Elevation Data 2010 (GMTED2010). 26. US Department of the Interior, US Geological Survey.

Dong, Z., Liu, H., Hu, H., Khan, M.Y.A., Wen, J., Chen, L., Tian, F., 2022. Future projection of seasonal drought characteristics using CMIP6 in the Lancang-Mekong River Basin. J. Hydrol. 610, 127815.

Duan, K., Mei, Y., 2014. Comparison of meteorological, hydrological and agricultural drought responses to climate change and uncertainty assessment. Water Resour. Manag. 28 (14), 5039–5054.

Ficklin, D.L., Luo, Y., Luedeling, E., Zhang, M., 2009. Climate change sensitivity assessment of a highly agricultural watershed using SWAT. J. Hydrol. 374 (1–2), 16–29.

Food and Agriculture Organization (FAO), 2005. Southeast Asia: Drought and Onset of the 2005 Rainy Season. Press Release by the Food and Agricultural Organization of the United nations, 29 April 2005. http://www.fao.org/Giews/english/shortnews/asiamekong050429.htm.

Ford, T.W., Labosier, C.F., 2017. Meteorological conditions associated with the onset of flash drought in the eastern United States. Agric. For. Meteorol. 247, 414–423.

Ford, T.W., McRoberts, D.B., Quiring, S.M., Hall, R.E., 2015. On the utility of in situ soil moisture observations for flash drought early warning in Oklahoma, USA. Geophys. Res. Lett. 42 (22), 9790–9798.

Franchini, M., Pacciani, M., 1991. Comparative analysis of several conceptual rainfall-runoff models. J. Hydrol. 122 (1–4), 161–219.

Funk, C., Peterson, P., Landsfeld, M., Pedreros, D., Verdin, J., Shukla, S., Husak, G., Rowland, J., Harrison, L., Hoell, A., Michaelsen, J., 2015. The climate hazards infrared precipitation with stations—a new environmental record for monitoring extremes. Sci. Data 2 (1), 1–21.

Grillakis, M.G., 2019. Increase in severe and extreme soil moisture droughts for Europe under climate change. Sci. Total Environ. 660, 1245–1255.

Gringorten, I.I., 1963. A plotting rule for extreme probability paper. J. Geophys. Res. 68 (3), 813–814.

Guo, H., Bao, A., Liu, T., Ndayisaba, F., He, D., Kurban, A., De Maeyer, P., 2017. Meteorological drought analysis in the lower Mekong Basin using satellite-based long-term CHIRPS product. Sustainability 9 (6), 901.

Hao, Z., AghaKouchak, A., 2013. Multivariate standardized drought index: a parametric multi-index model. Adv. Water Resour. 57, 12–18.

Hao, Z., AghaKouchak, A., 2014. A nonparametric multivariate multi-index drought monitoring framework. J. Hydrometeorol. 15 (1), 89–101.

Hao, Z., AghaKouchak, A., Nakhjiri, N., Farahmand, A., 2014. Global integrated drought monitoring and prediction system. Sci. Data 1 (1), 1–10.

Harris, I., Osborn, T.J., Jones, P., Lister, D., 2020. Version 4 of the CRU TS monthly high-resolution gridded multivariate climate dataset. Sci. Data 7 (1), 1–18.

Hempel, S., Frieler, K., Warszawski, L., Schewe, J., Piontek, F., 2013. A trend-preserving bias correction–the ISI-MIP approach. Earth Syst. Dyn. 4 (2), 219–236.

Hobbins, M.T., Wood, A., McEvoy, D.J., Huntington, J.L., Morton, C., Anderson, M., Hain, C., 2016. The evaporative demand drought index. Part I: linking drought evolution to variations in evaporative demand. J. Hydrometeorol. 17 (6), 1745–1761.

Jing, W., Zhao, X., Yao, L., Jiang, H., Xu, J., Yang, J., Li, Y., 2020. Variations in terrestrial water storage in the Lancang-Mekong river basin from GRACE solutions and land surface model. J. Hydrol. 580, 124258.

Kang, H., Sridhar, V., 2017. Combined statistical and spatially distributed hydrological model for evaluating future drought indices in Virginia. J. Hydrol. Reg. Stud. 12, 253–272.

Kang, H., Sridhar, V., 2018. Improved drought prediction using near real-time climate forecasts and simulated hydrologic conditions. Sustainability 10 (6), 1799.

Kang, H., Sridhar, V., 2019. Drought assessment with a surface-groundwater coupled model in the Chesapeake Bay watershed. Environ. Model. Softw. 119, 379–389. https://doi.org/10.1016/j.envsoft.2019.07.002.

Kang, H., Sridhar, V., 2020. A novel approach combining simulated soil moisture and stochastic techniques to forecasting drought in the Mekong River basin. Int. J. Climatol. https://doi.org/10.1002/joc.6860.

Kang, H., Sridhar, V., 2021. A near-term drought assessment using hydrological and climate forecasting in the Mekong River basin. Int. J. Climatol. 41, E2497–E2516.

Kang, H., Sridhar, V., Mills, B.F., Hession, W.C., Ojego, J.A., 2019. Economy-wide climate change impacts on green water droughts based on the hydrologic simulations. Agric. Syst. 171, 76–88.

Kang, H., Sridhar, V., Mainuddin, M., Trung, L.D., 2021. Future rice farming threatened by drought in the lower Mekong Basin. Sci. Rep. 11 (1), 1–15.

Keoviilignavong, O., Nguyen, T.H., Hirsch, P., 2021. Reviewing the causes of Mekong drought before and during 2019–20. Int. J. Water Resour. Dev. 1–21.

Li, C., Fang, H., 2021. Assessment of climate change impacts on the streamflow for the Mun River in the Mekong Basin, Southeast Asia: using SWAT model. Catena 201, 105199.

Li, H., Wu, H., Huang, M., Leung, L., 2012. Representing natural and manmade drainage systems in an earth system modeling framework. Irrig. Drain. Syst. Eng 1, 1–2.

Li, Y., Lu, H., Yang, K., Wang, W., Tang, Q., Khem, S., Yang, F., Huang, Y., 2021. Meteorological and hydrological droughts in Mekong River basin and surrounding areas under climate change. J. Hydrol. Reg. Stud. 36, 100873.

Liang, X., Lettenmaier, D.P., Wood, E.F., Burges, S.J., 1994. A simple hydrologically based model of land surface water and energy fluxes for general circulation models. J. Geophys. Res. Atmos. 99 (D7), 14415–14428.

Lu, Y., Tian, F., Guo, L., Borzì, I., Patil, R., Wei, J., Liu, D., Wei, Y., Yu, D.J., Sivapalan, M., 2021. Socio-hydrologic modeling of the dynamics of cooperation in the transboundary Lancang-Mekong River. Hydrol. Earth Syst. Sci. 25 (4), 1883–1903.

Mao, Y., Nijssen, B., Lettenmaier, D.P., 2015. Is climate change implicated in the 2013–2014 California drought? A hydrologic perspective. Geophys. Res. Lett. 42 (8), 2805–2813.

McEvoy, D.J., Huntington, J.L., Hobbins, M.T., Wood, A., Morton, C., Anderson, M., Hain, C., 2016. The evaporative demand drought index. Part II: CONUS-wide assessment against common drought indicators. J. Hydrometeorol. 17 (6), 1763–1779.

McKee, T.B., Doesken, N.J., Kleist, J., 1993, January. The relationship of drought frequency and duration to time scales. Proceedings of the 8th Conference on Applied Climatology. 17, 22, pp. 179–183.

Mishra, A.K., Singh, V.P., 2010. A review of drought concepts. J. Hydrol. 391 (1–2), 202–216.

Monteith, J.L., 1965. Evaporation and environment. Symposia of the Society for Experimental Biology. 19. Cambridge University Press, Cambridge, pp. 205–234.

Moriasi, D.N., Arnold, J.G., Van Liew, M.W., Bingner, R.L., Harmel, R.D., Veith, T.L., 2007. Model evaluation guidelines for systematic quantification of accuracy in watershed simulations. Trans. ASABE 50 (3), 885–900.

Moriasi, D.N., Gitau, M.W., Pai, N., Daggupati, P., 2015. Hydrologic and water quality models: performance measures and evaluation criteria. Trans. ASABE 58 (6), 1763–1785.

Moss, R.H., Babiker, M., Brinkman, S., Calvo, E., Carter, T., Edmonds, J.A., Elgizouli, I., Emori, S., Lin, E., Hibbard, K., Jones, R., 2008. Towards New Scenarios for Analysis of Emissions, Climate Change, Impacts, and Response Strategies.

MRC, 2005. Overview of the Hydrology of the Mekong Basin, Mekong River Commission, Vientiane Lao PDR.

MRC, 2010. State of the Basin Report 2010, Mekong River Commission, Vientiane, Lao PDR. (9) p.D05109.

Mukherjee, S., Mishra, A., Trenberth, K.E., 2018. Climate change and drought: a perspective on drought indices. Curr. Clim. Chang. Rep. 4 (2), 145–163.

Nguyen, H., Wheeler, M.C., Otkin, J.A., Cowan, T., Frost, A., Stone, R., 2019. Using the evaporative stress index to monitor flash drought in Australia. Environ. Res. Lett. 14 (6), 064016.

Noguera, I., Domínguez-Castro, F., Vicente-Serrano, S.M., 2021. Flash drought response to precipitation and atmospheric evaporative demand in Spain. Atmosphere 12 (2), 165.

Otkin, J.A., Anderson, M.C., Hain, C., Mladenova, I.E., Basara, J.B., Svoboda, M., 2013. Examining rapid onset drought development using the thermal infrared–based evaporative stress index. J. Hydrometeorol. 14 (4), 1057–1074.

Otkin, J.A., Anderson, M.C., Hain, C., Svoboda, M., 2014. Examining the relationship between drought development and rapid changes in the evaporative stress index. J. Hydrometeorol. 15 (3), 938–956.

Otkin, J.A., Svoboda, M., Hunt, E.D., Ford, T.W., Anderson, M.C., Hain, C., Basara, J.B., 2018. Flash droughts: a review and assessment of the challenges imposed by rapid-onset droughts in the United States. Bull. Am. Meteorol. Soc. 99 (5), 911–919.

Parker, T., Gallant, A., Hobbins, M., Hoffmann, D., 2021. Flash drought in Australia and its relationship to evaporative demand. Environ. Res. Lett. 16 (6), 064033.

Real-Rangel, R.A., Pedrozo-Acuña, A., Breña-Naranjo, J.A., Alcocer-Yamanaka, V.H., 2018. Novel drought hazard monitoring framework for decision support under data scarcity. EPiC Series in Engineering. 3, pp. 1744–1751.

Ruiz-Barradas, A., Nigam, S., 2018. Hydroclimate variability and change over the Mekong River basin: modeling and predictability and policy implications. J. Hydrometeorol. 19 (5), 849–869.

Sam, T.T., Khoi, D.N., Thao, N.T.T., Nhi, P.T.T., Quan, N.T., Hoan, N.X., Nguyen, V.T., 2019. Impact of climate change on meteorological, hydrological and agricultural droughts in the Lower Mekong River Basin: a case study of the Srepok Basin, Vietnam. Water Environ. J. 33 (4), 547–559.

Sanchez, P.A., Ahamed, S., Carré, F., Hartemink, A.E., Hempel, J., Huising, J., Lagacherie, P., McBratney, A.B., McKenzie, N.J., de Lourdes Mendonça-Santos, M., Minasny, B., 2009. Digital soil map of the world. Science 325 (5941), 680–681.

Shaw, R., Nguyen, H. (Eds.), 2011. Droughts in Asian Monsoon Region. Emerald Group Publishing.

van der Schrier, G., Barichivich, J., Briffa, K.R., Jones, P.D., 2013. A scPDSI-based global data set of dry and wet spells for 1901–2009. J. Geophys. Res. Atmos. 118 (10), 4025–4048.

Schwalm, C.R., Glendon, S., Duffy, P.B., 2020. RCP8. 5 tracks cumulative CO2 emissions. 117 (33), 19656–19657.

Seong, C., Sridhar, V., Billah, M.M., 2018. Implications of potential evapotranspiration methods for streamflow estimations under changing climatic conditions. Int. J. Climatol. 38 (2), 896–914.

Sheffield, J., Wood, E.F., 2012. Drought: Past Problems and Future Scenarios. Routledge.

Sheffield, J., Goteti, G., Wood, E.F., 2006. Development of a 50-year high-resolution global dataset of meteorological forcings for land surface modeling. J. Clim. 19 (13), 3088–3111.

Sheffield, J., Wood, E.F., Roderick, M.L., 2012. Little change in global drought over the past 60 years. Nature 491 (7424), 435–438.

Soukhaphon, A., Baird, I.G., Hogan, Z.S., 2021. The impacts of hydropower dams in the Mekong River basin: a review. Water 13 (3), 265.

Sridhar, V., Wedin, D.A., 2009. Hydrological behaviour of grasslands of the Sandhills of Nebraska: water and energy-balance assessment from measurements, treatments, and modelling. Ecohydrology 2 (2), 195–212.

Sridhar, V., Jaksa, W.T.A., Fang, B., Lakshmi, V., Hubbard, K.G., Jin, X., 2013. Evaluating bias-corrected AMSR-E soil moisture using in situ observations and model estimates. Vadose Zone J. 12 (3), vzj2013-05.

Sridhar, V., Kang, H., Ali, S.A., 2019. Human-induced alterations to land use and climate and their responses for hydrology and water management in the Mekong River basin. Water 11 (6), 1307.

Sridhar, V., Ali, S.A., Sample, D.J., 2021. Systems analysis of coupled natural and human processes in the Mekong River basin. Hydrology 8 (3), 140.

Stanke, C., Kerac, M., Prudhomme, C., Medlock, J., Murray, V., 2013. Health effects of drought: a systematic review of the evidence. PLoS Curr. 5.

Svoboda, M., LeComte, D., Hayes, M., Heim, R., Gleason, K., Angel, J., Rippey, B., Tinker, R., Palecki, M., Stooksbury, D., Miskus, D., 2002. The drought monitor. Bull. Am. Meteorol. Soc. 83 (8), 1181–1190.

Swenson, S., Wahr, J., 2006. Post-processing removal of correlated errors in GRACE data. Geophys. Res. Lett. 33 (8).

Tatsumi, K., Yamashiki, Y., 2015. Effect of irrigation water withdrawals on water and energy balance in the Mekong River Basin using an improved VIC land surface model with fewer calibration parameters. Agric. Water Manag. 159, 92–106.

Thilakarathne, M., Sridhar, V., 2017. Characterization of future drought conditions in the lower Mekong River basin. Weather Clim. Extremes 17, 47–58.

Thomson, A.M., Calvin, K.V., Smith, S.J., Kyle, G.P., Volke, A., Patel, P., Delgado-Arias, S., Bond-Lamberty, B., Wise, M.A., Clarke, L.E., Edmonds, J.A., 2011. RCP4. 5: a pathway for stabilization of radiative forcing by 2100. Clim. Chang. 109 (1), 77–94.

Trenberth, K.E., Dai, A., Van Der Schrier, G., Jones, P.D., Barichivich, J., Briffa, K.R., Sheffield, J., 2014. Global warming and changes in drought. Nat. Clim. Chang. 4 (1), 17–22.

USDA (U.S. Department of Agriculture), 1972. Soil Conservation Service, National Engineering Handbook; Hydrology (Section 4, Chapters 4–10). GPO, Washington, DC, USA.

USGS, 2021. USGS EROS Archive—Land Cover Products—Global Land Cover Characterization (GLCC). https://www.usgs.gov/centers/eros/science/usgs-eros-archive-land-cover-products-global-land-cover-characterization-glcc?qt-science_center_objects=0#qt-science_center_objects Accessed 2021.

Västilä, K., Kummu, M., Sangmanee, C., Chinvanno, S., 2010. Modelling climate change impacts on the flood pulse in the Lower Mekong floodplains. J. Water Clim. Chang. 1 (1), 67–86.

VNE (VNExpress International), 2016. Historic Drought Costs Vietnam $670 Million. VNExpress International Retrieved from https://e.vnexpress.net/news/news/historic-drought-costs-vietnam-670-million-3412536.html.

Wang, D., Hejazi, M., Cai, X., Valocchi, A.J., 2011. Climate change impact on meteorological, agricultural, and hydrological drought in Central Illinois. Water Resour. Res. 47 (9).

Westerling, A.L., Hidalgo, H.G., Cayan, D.R., Swetnam, T.W., 2006. Warming and earlier spring increase western US forest wildfire activity. Science 313 (5789), 940–943.

WFP, 2009. Poverty and Vulnerabilities in Cambodia. Powerpoint Presentation by Jean Pierre de Margerie at National Forum on Food Security and Nutrition, Cambodia, 6 July, 2009.

Wipatayotin, A., 2016. Drought may result in B62bn in damages: Farmers face high cost of water scarcity crisis. Bangkok Post. Retrieved from https://www.bangkokpost.com/thailand/general/849356/drought-may-result-in-b62bn-in-damages.

Wood, E.F., Lettenmaier, D.P., Zartarian, V.G., 1992. A land-surface hydrology parameterization with subgrid variability for general circulation models. J. Geophys. Res. Atmos. 97 (D3), 2717–2728.

Xu, K., Yang, D., Yang, H., Li, Z., Qin, Y., Shen, Y., 2015. Spatio-temporal variation of drought in China during 1961–2012: a climatic perspective. J. Hydrol. 526, 253–264.

Yuan, X., Wang, L., Wu, P., Ji, P., Sheffield, J., Zhang, M., 2019. Anthropogenic shift towards higher risk of flash drought over China. Nat. Commun. 10 (1), 1–8.

Yue, S., Ouarda, T.B., Bobée, B., Legendre, P., Bruneau, P., 1999. The Gumbel mixed model for flood frequency analysis. J. Hydrol. 226 (1–2), 88–100.

Zhang, X., Liu, H., 2020. Analysis of drought character in the Mekong River basin. Flood Prevention and Drought Relief in Mekong River Basin. Springer, Singapore, pp. 95–107.

Zhang, X., Xu, Y.P., Fu, G., 2014. Uncertainties in SWAT extreme flow simulation under climate change. J. Hydrol. 515, 205–222.

Zhang, X., Qu, Y., Ma, M., Liu, H., Su, Z., Lv, J., Peng, J., Leng, G., He, X., Di, C., 2020. Satellite-based operational real-time drought monitoring in the transboundary Lancang-Mekong River basin. Remote Sens. 12 (3), 376.

Zhou, T., Haddeland, I., Nijssen, B., Lettenmaier, D.P., 2016. Human-induced changes in the global water cycle. Terrestrial Water Cycle and Climate Change: Natural and Human-Induced Impacts. Geophys. Monogr. Ser. https://doi.org/10.1002/9781118971772.ch4.